VIBRATION ANALYSIS OF CARBON NANOTUBES USING CONTINUUM MODEL AND FINITE ELEMENT MODEL

by

HARI SUBRAMANIAM
B.E. Bharathair University, India 2002

A thesis submitted in partial fulfillment of the requirements
for the degree of Master of Science
from the Department of Mechanical, Materials and Aerospace Engineering
in the College of Engineering and Computer Science
at the University of Central Florida
Orlando, Florida

Fall Term
2005

ABSTRACT

The main objective of the thesis is to propose the methods of determining vibration behavior of carbon nanotubes (CNTs) using continuum models and finite element models. Secondary objective is to find the effect of van der Waals force on vibration of multiwalled carbon nanotubes . The study of vibration behavior of CNTs is important because of their potential engineering applications such as nano-mechanical resonators and tips of scanning probe instruments where they are subjected to mechanical vibrations. Continuum modeling is based on an elastic beam model. The interlayer van der Waals interactions are represented by Lennard-Jones potential. In finite element modeling, single walled nanotubes (SWNTs) are modeled as finite beam elements and multi-walled nanotubes (MWNTs) as finite solid elements. The interlayer van der Waals interactions are simulated by distributed springs. The proposed finite element approach and continuum approach for vibration analysis of CNTs are verified by comparing the results with experimental and analytical results available in the literature. The results from both continuum and finite element modeling show that the effect of van der Waals force on vibration of MWNTs are high for smaller aspect ratios irrespective of boundary conditions and number of layers; fixed nanotube than cantilever nanotube for the same dimensions ; five-walled nanotube than a double walled nanotube for the same aspect ratio.

ACKNOWLEDGMENTS

I would like to take this opportunity to express my sincere appreciation to my professor and advisor, Dr. Quan A. Wang, who has helped and guided me throughout this research.

I am grateful to Dr. David Nicholson who taught me finite element techniques and Dr. Richard P. Zarda who taught me the skills in finite element modeling. I would like to thank Dr. Ranganathan Kumar who helped with financial assistantship for my graduate studies.

I would also like to thank my thesis defense committee members; Dr. Kuo-Chi "Kurt" Lin and Dr. Gangyi Zhou. Last but not least, I would like to thank my parents, my family and my friends' for their enduring support in my academic pursuit.

TABLE OF CONTENTS

LIST OF FIGURES

LIST OF TABLES

CHAPTER 1 INTRODUCTION

DREXLER says, “Coal and diamonds, sand and computer chips, cancer and healthy tissues: throughout the history, variations in the arrangement of atoms have distinguished the cheap from the cherished, the diseased from the healthy. Arranged one way the atoms make up soil, air and water: arranged other they make ripe strawberries. Arranged one way they make up homes and fresh air, arranged another they make up ash and smoke! Our ability to arrange atoms lies at the foundation of nanotechnology”

Iijima discovered CNTs in 1991. The prefix “nano” corresponds to a basic unit on a length scale, meaning 10^{-9} meters, which is a hundred to a thousand times smaller than a typical biological cell or bacterium. At the nanometer length scale, the dimensions of the materials and devices begin to reach the limit of 10 to 100s of atoms, wherein entirely new physical and chemical effects are observed; and possibilities arise for the next generation of cutting-edge products based on the ultimate miniaturization or so called “nanoization” of the technology. CNTs have a variety of applications because of their distinctive molecular structure and their fascinating mechanical and electrical properties.

1.1 Structure of CNTs

The structure of CNTs can be considered as arising from the folding of one or more layers of graphite to form a cylinder composed of carbon hexagons. These nanotubes have a hemispherical "cap" at each end of the cylinder as shown in the figure I. They are light, flexible, thermally stabile, and are chemically inert.

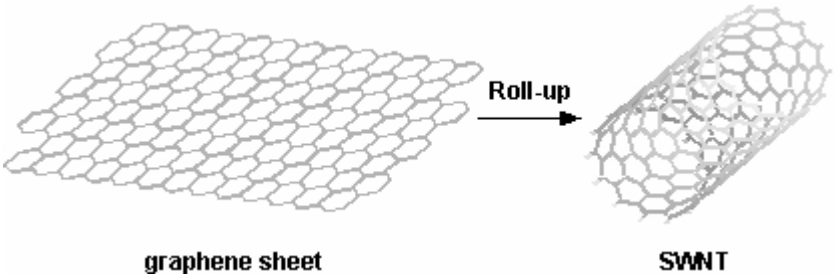

Figure I Single Walled CNT

Nanotubes are composed entirely of sp2 bonds, which are stronger than the sp3 bonds found in diamond. This bonding structure provides them with their unique strength. Nanotubes align themselves into ropes held together by van der Waals force. Under high pressure, nanotubes can merge together, trading some sp2 bonds for sp3 bonds, giving great possibility for producing strong, unlimited-length wires through high-pressure nanotubes linking.

1.1.1 Types of CNTs

Basically nanotubes are two types depending upon the layers as shown in figure II. They are

1. Single walled nanotube (SWNT)
2. Multi walled nanotube (MWNT)

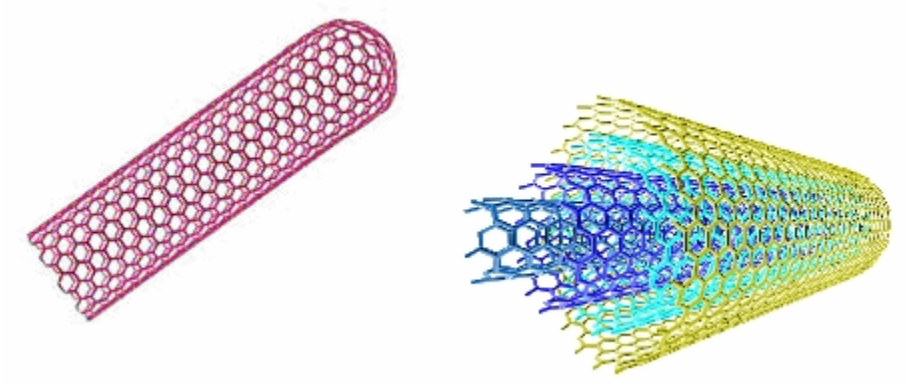

Figure II Single and Multi Walled Nanotube

Nanotubes can be categorized into three types according to their structure. They are

1. Arm-Chair
2. Chiral
3. Zigzag

Nanotubes form different types, which can be described by the chiral vector (n, m), where n and m are integers of the vector equation $C_h = na_1 + ma_2$. The chiral vector is determined as shown by the figure III.

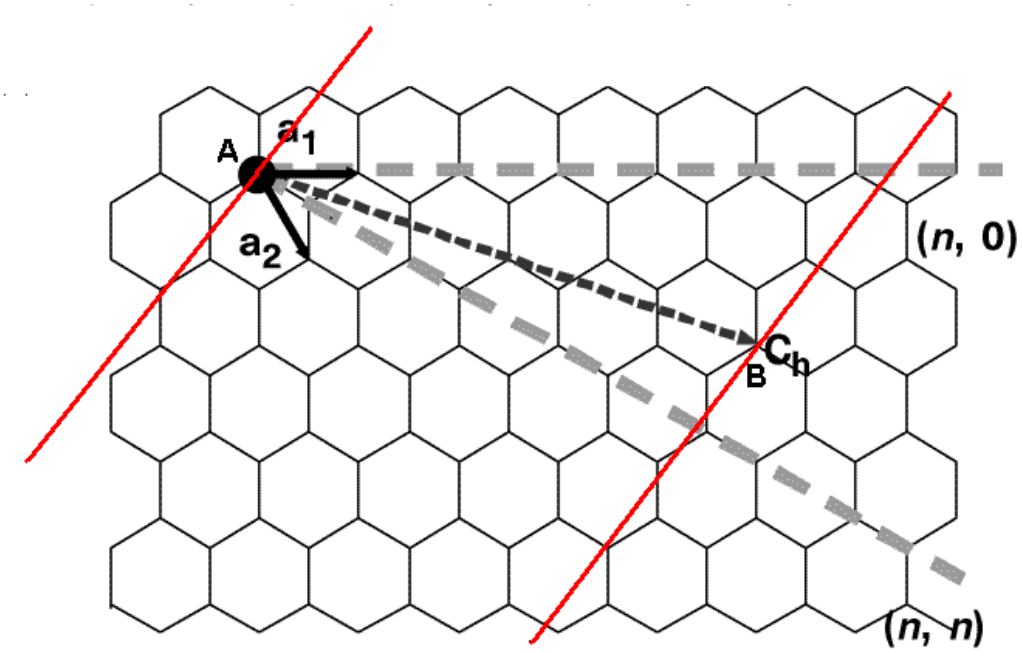

Figure III Chiral Vector of a Nanotube

Imagine that the nanotube is unraveled into a planar sheet. Draw two continuous lines along the tube axis where the separation takes place. In other words, if we cut along the two continuous solid lines and then match their ends together in a cylinder, you get the nanotube that you started with. Now, find any point on one of the red lines that intersects one of the carbon atoms (point A). Next, draw the Armchair line (n, n) which travels across each hexagon, separating them into two equal halves. Now that you have the armchair line drawn, find a point along the other tube axis that intersects a carbon atom nearest to the Armchair line (point B). Now connect A and B with our chiral vector C_h .The wrapping angle; (not shown) is formed between C_h and the Armchair line. If C_h lies along the Armchair line (=0°), then it is called an "Armchair" nanotube. If =30°, then the tube is of the "zigzag" type. Otherwise, if 0°<<30° then it is a "chiral" tube. The

values of n and m determine the chirality, or "twist" of the nanotube. The chirality in turn affects the conductance of the nanotube, its density, its lattice structure, and other properties. Figure IV shows the different types of carbon nanotubes according to their structure.

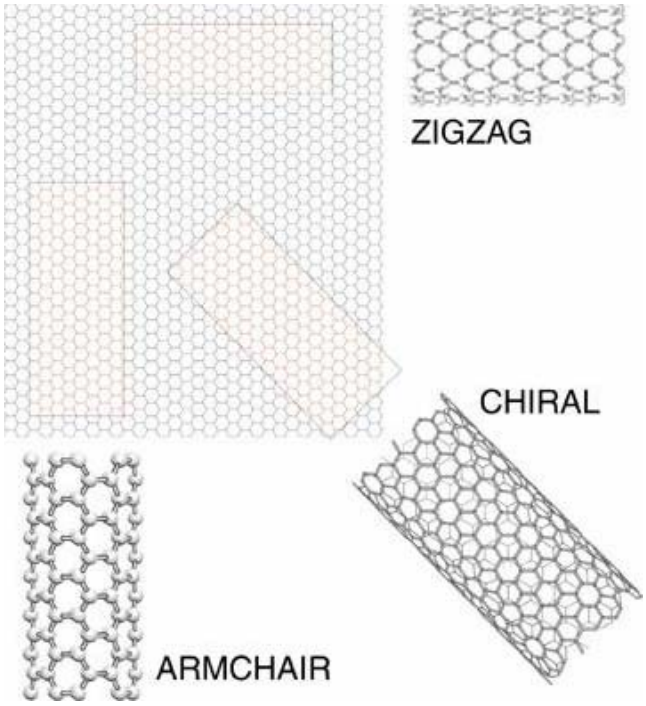

Figure IV Types of Single Walled CNTs

1.2 Manufacture of CNTs

CNTs can be manufactured by the following methods

a. Arc discharge
b. Laser Ablation
c. Chemical Vapour Deposition

Arc discharge involves an electrical discharge from a carbon-based electrode in a suitable atmosphere to produce both single and multi-wall tubes of high quality but in low quantities. Laser ablation uses a high-power laser to vaporise a graphite source loaded with a metal catalyst. The carbon in the graphite reforms as predominantly single-wall nanotubes on the metal catalyst particles.

Chemical vapour deposition (CVD) is where a hydrocarbon feedstock is reacted with a suitable metal-based catalyst in a hot furnace to 'grow' nanotubes which are subsequently removed from the substrate and catalyst by a simple acid wash. In a typical chemical vapor deposition process the substrate is exposed to one or more volatile precursors, which react and/or decompose on the substrate surface to produce the desired deposit. The chemical vapor deposition method has shown the most promise in being able to produce larger quantities of nanotube (compared to the other methods) at lower cost.

1.3 Applications of CNTs

CNTs exhibit unique electronic and mechanical properties because of their curvature. Because of their inimitable properties, CNTs find a number of interesting applications in different fields of engineering. Some of the applications discussed by Ajayan et al. (2001) are as follows

a. Carbon nanotubes have the right combination of properties – nanometer size diameter, structural integrity, high electrical conductivity, and chemical stability – that makes good electron emitters.
b. Prototype matrix-addressable diode flat panel displays can be fabricated using CNTs as the electron emission source.
c. Nanotubes can be used as reinforcements in composite materials. Nanotube reinforcements will increase the toughness of the composites by absorbing energy during their highly flexible elastic behavior.
d. Nanotube filled polymers can be used in electromagnetic induction (EMI) shielding applications.
e. Because of its hollow geometry and nano scale diameter, it has been predicted that the carbon nanotubes can store liquid and gas in the inner cores through a capillary effect.
f. CNT's because of their extremely small sizes, high conductivity, high mechanical strength and flexibility, they are used in STM, AFM instruments as well as other scanning probe instruments, such as an electrostatic force microscope.
g. MWNT and SWNT tips were used in a tapping mode to image biological molecules such as amyloid-b-protofibrils with resolution never achieved before.
h. Nanotubes with controlled helicities could be used as unique probes for molecular recognition, based on the helicity and dimensions, which are recognized by organic molecules of comparable length scales.
i. CNTs have relatively straight and narrow channels in their cores which can be filled with foreign materials to fabricate one-dimensional nanowires.

j. Since the electrical resistivities of SNWTs were found to change sensitively on exposure to gaseous ambient, hence CNTs can be used as chemical sensors.

They can be used to dissipate heat from tiny computer chips. Nanotube composite motor brushes are better lubricated, stronger and more accurately moldable. CNTs have already been used as composite fibers in polymers and concrete to improve their mechanical, thermal and electrical properties of the bulk product. Nanotubes are critical material that enables construction of space elevators from earth to geosynchronous orbit.

Gao et al., (2000) found that CNTs have the highest reversible capacity of any carbon material for use in lithium-ion batteries. Because of their negligible weight, they find application in space applications. Since nanotubes are similar scale size of DNA, promising possibilities can be expected by introducing them to reinforce tissue scaffolds. CNTs have a high surface area and their ability to attach to any chemical species to their sidewalls provides an opportunity for unique catalyst supports.

CHAPTER 2 LITERATURE REVIEW

2.1 Literature Review on Modeling Techniques

Extensive research has been carried out in the field of nanotubes. The first method that has been used by researchers to study the properties of CNTs is experimental method (Poncharal et al., 1999; Krishnan et al., 1998). Though the experimental method gave accurate results, it is very time consuming and costlier. The second method that has been used by researchers is atomic modeling like molecular dynamics (Iijma et al., 1996) since nanoeffects and accurate solutions for nano-scale size problems are possible by this modeling. But Molecular Dynamic (MD) simulations are only limited to systems with a smaller number of molecules and atoms. So only single walled nanotubes with small size can be simulated using molecular dynamics.

The third method that has been used by researchers in studying CNT is continuum modeling (Yakobson et al., 1996; Ru et al., 2000; Yoon et al., 2002; Wang et al., 2005). The main issue in studying CNTs using continuum models was determining the bulk properties (at macroscopic level) corresponding to molecular properties of CNT. Wang et al. (2005) explored and developed benchmark for the applicability of shell model and beam model in CNT stability results. They also proposed an independent flexural stiffness constant of a nanotube when elastic beam model is used. Ru et al. (2000) used a continuum beam model to study the column buckling of nanotube. Yakobson et al. (1996) used a continuum shell model to study buckling of nanotubes.

Different types of CNT models such as molecular dynamics model, continuum shell model and continuum solid model are shown in the figure V.

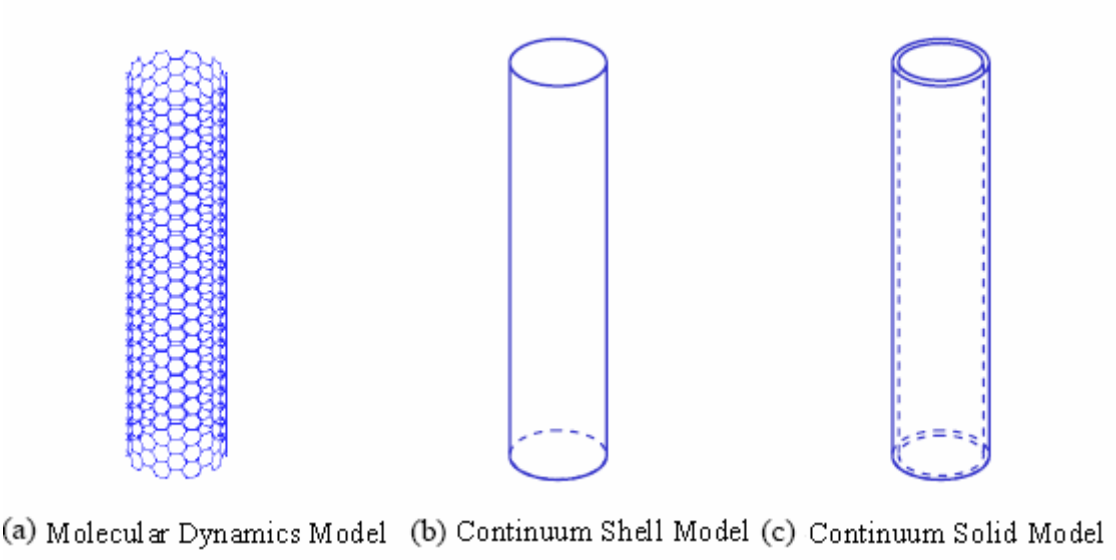

Figure V Types of Modeling of CNTs

Harik et al. (2002) studied about the applicability of continuum beam models for studying the behaviors of CNTs. He concluded that continuum beam model can be used for the qualitative analysis of CNTs when the ratio of length and diameter of nanotube is greater than 10. As the number of walls of CNTs increases it becomes complex to study its behavior using experiments, molecular dynamics and continuum models.

The fourth method that has been used by researchers in studying CNT is finite element method. Very little work had been done in the field of finite element analysis of CNTs. Pantano et al. (2003) modeled individual tubes as shell finite elements and the effects of van der Waals forces were simulated using special interaction elements. He studied the mechanics of

wrinkling of multiwalled CNTs demonstrating the role of multiwalled shell structure and interwall van der Waals interactions in governing bucking and postbuckling behavior. Liu et al. (2004) used a solid cylindrical finite element model for studying the rippling of a nanobeam under pure bending.

2.2 Need for Vibration Analysis

CNTs are widely used as tips of AFM, STM instruments as well as other scanning probe instrument. As the nanotube tip touches the sample, it induces mechanical vibrations. Hence there is a greater need to study the vibration behavior of single and multi walled CNTs. CNTs are also used as nanomechanical resonators. Snow et al (2002) studied the stability of imaging using single-wall CNTs as probes for atomic force microscopy. They suggested that thicker, multiwalled probes or very short single-wall probes extending from nanotube bundles might be better for imaging highly textured surfaces.

2.3 Literature Review on Vibration Analysis of CNTs

Researchers have been using two methods to study the vibration behavior of CNTs namely experimental method and continuum modeling method. Poncharal et al., 1999 and Krishnan et al., 1998 used experimental method. Poncharal et al. (1999) measured the fundamental resonance frequency of multiwalled CNTs induced by an alternating electric field in a transmission electron microscope and they then calculated the axial elastic modulus using the modulus frequency

relation resulting from the classical analysis of linear elasticity for cantilevered beams. Krishnan et al. (1998) estimated the stiffness of single walled CNTs by observing their free standing room temperature vibrations in a transmission on electron microscope. The nanotube dimensions and vibration amplitude were measured from electron micrographs and it was assumed that the vibration modes were driven stochastically and were chosen of a clamped cantilever.

Yoon et al. (2002) and Wang et al. (2005) used continuum models for studying vibration behavior of CNTs. Yoon et al. (2002) used a multiple elastic model to study vibration behaviors of double and five-walled nanotube. They calculated non-coaxial resonant frequencies and the associated non-coaxial vibration modes. They found that the first few noncoaxial resonant frequencies are found to be insensitive to vibration modes, length of MWNT's and the end conditions, while they decrease with the number of nested layers. They also found that internal non-coaxial resonance will be excited at the high natural frequencies, and MWNT's cannot maintain their concentric structure at ultra high frequencies. Wang et al. (2005) found the frequencies of cantilever SWNT and compared the results with the experimental results of Krishnan et al. (1998).

2.4 Proposed Research

The research in this thesis proposes two effective methods of determining natural frequencies of SWNT's and MWNT's. The first method is using continuum model. The proposed continuum model unlike continuum model of Yoon et al. (2002) doesn't use straight normal postulate for finding the bending rigidity of CNT instead it calculates the bending rigidity by the method proposed by Wang et al. (2005).

The second method proposed for determining natural frequencies of CNTs is finite element modeling, where single walled nanotubes (SWNTs) are modeled as finite beam elements and multi-walled nanotubes (MWNTs) as finite solid elements. The proposed finite element model for MWNT is simple and effective. The model is simple because the van der Waals force is simulated using distributed springs and the model is effective because it also predicts the effect of van der Waals force on vibration of MWNTs.

CHAPTER 3 CONTINUUM MODELING

3.1 Introduction

CNTs can be considered as Euler-Bernoulli beam to study its vibration behavior. According to Euler-Bernoulli beam theory, the equation of motion for a forced vibration of a uniform beam as shown in figure VI is given by

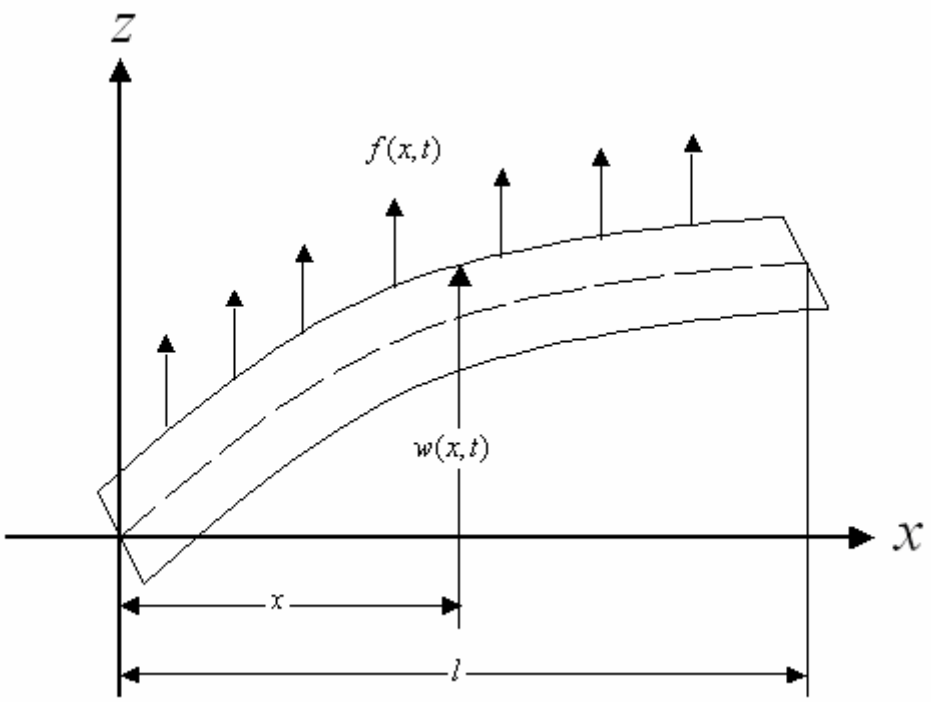

Figure VI A beam in bending

$$E_b I_b \frac{\partial^4 w_b(x,t)}{\partial x^4} + \rho_b A_b \frac{\partial^2 w_b(x,t)}{\partial x^2} = f_b(x,t) \qquad (1)$$

Where E_b is the young's modulus, I_b is the moment of inertia of the beam cross-section about y-axis, ρ_b is the mass density, $f_b(x,t)$ is the external force, $w_b(x,t)$ is the flexural deflection of the beam and A is the area of the cross-section of the beam.

The governing equation for a SWNT to study its natural frequencies is given from Euler-Bernoulli beam model when $f(x,t) = 0$ (no external force) is substituted in eq (1)

$$EI\frac{\partial^4 w(x,t)}{\partial x^4} + \rho A\frac{\partial^2 w(x,t)}{\partial x^2} = 0. \qquad (2)$$

Where E is the young's modulus of SWNT, I is the moment of inertia of SWNT, ρ is the mass density of SWNT, $w(x,t)$ is the flexural deflection of SWNT and A is the area of the cross-section of SWNT

For a MWNT, a multiple elastic beam model is suggested in which each of the nested nanotubes is described as an individual elastic beam and the deflections of all nested tubes are coupled through the van der Waals interaction between any two adjacent tubes. The force term is given by product of van der Waals interaction co-efficient and the deflection. The governing equations for a MWNT from Euler-Bernoulli beam model are given by

$$c_1(w_2 - w_1) = EI_1\frac{\partial^4 w_1}{\partial x^4} + \rho A_1\frac{\partial^2 w_1}{\partial t^2} \qquad (3a)$$

$$c_2(w_3 - w_2) - c_1(w_2 - w_1) = EI_2\frac{\partial^4 w_2}{\partial x^4} + \rho A_2\frac{\partial^2 w_2}{\partial t^2} \qquad (3b)$$

……

$$-c_{N-1}(w_N - w_{N-1}) = EI_N \frac{\partial^4 w_N}{\partial x^4} + \rho A_N \frac{\partial^2 w_N}{\partial t^2} \quad (3c)$$

where subscript 1,2 and N stand for the variables in first (innermost) tube, second tube and the N^{th} tube. Where E is the young's modulus of CNT, ρ is the mass density of CNT, I_N is the moment of inertia of N^{th} CNT, w_N is the flexural deflection of N^{th} CNT and A_N is the area of the cross-section of N^{th} CNT, c_N is the van der Waals force between N^{th} CNT and $(N+1)^{th}$ CNT.

3.2 Bulk Properties of CNTs

3.2.1 Van der Waals Force

The multiple layers of graphite sheets in a multi walled CNTs are held together by van der Waals forces. The van der Waals force is a non-bonded interaction, and it can be an attraction force or a repulsion force. The attraction occurs when a pair of atoms approaches each other within a certain distance. The repulsion occurs when the distance between the interacting atoms becomes less than the sum of their contact radii. The van der Waals force is modeled using Lennard-Jones potential.

van der Waals force (c_1)between first (innermost) tube and second tube is given by

$$c_1 = (2r_i)x\left[\frac{\partial^2 V(r)}{\partial r^2}\right]x\rho \tag{4}$$

where r_i is the inter-atomic distance, $V(r)$ is Lennard-Jones Potential and ρ is the density.

Lennard-Jones Potential gives the potential energy between two physically interacting non-bonded carbon atoms in graphite. Lennard-Jones Potential is given by

$$V(r) = 4\varepsilon\left[\left(\frac{\sigma}{r}\right)^{12} - \left(\frac{\sigma}{r}\right)^{6}\right] \tag{5}$$

where σ, ε are Lennard-Jones constants

$\varepsilon = 2.968E-03ev$

$\sigma = 3.407A^0$

r is the distance between two atoms having the Lennard-Jones interaction.

The Lennard-Jones Potential is differentiated twice with respect to inter-atomic distance (r)

$$\frac{\partial V}{\partial r} = 4\varepsilon\left[-12\sigma^{12}r^{-13} + 6\sigma^{6}r^{-7}\right] \tag{6}$$

$$\frac{\partial^2 V}{\partial^2 r} = 4\varepsilon\left[156\sigma^{12}r^{-14} - 42\sigma^{6}r^{-8}\right] \tag{7}$$

$$= 4\varepsilon\left[156\frac{\sigma^{12}}{r^{14}} - 42\frac{\sigma^{6}}{r^{6}}\right] \tag{8}$$

$$\frac{\partial^2 V}{\partial^2 r}_{@r=0.34E-09} = 4x2.968E-03x\left[156\frac{(3.407E-10)^{12}}{(0.34E-09)^{14}} - 42\frac{(3.407E-10)^{6}}{(0.34E-09)^{6}}\right] \quad (9)$$

$$= 1.2054\text{E}19 \text{ ev/m}^2 \quad (10)$$

The density is given by

$$\rho = \left[\frac{4sqrt(3)}{9r^2}\right] \quad (11)$$

Substituting eq (10) and eq (11) in eq (4), van der Waals force between innermost tube (d_i) and outer tube (d_o) is given by

$$c_1 = 2r_i\left[\frac{\partial^2 V}{\partial\ r^2}\right]x\left[\frac{4sqrt(3)}{9r^2}\right] = 2.0647\text{x}10^{20}(\frac{d_o + d_i}{2})\ \text{N/m}^2 \quad (12)$$

3.2.2 Bending Rigidity

Krishnan et al., (1998) used the straight normal postulate to calculate the bending stiffness of nanotubes. Straight normal postulate states that the longitudinal deformation at any point in the flexural direction is proportional to the distance between that point to the mid-plane of mid-surface of the structure). However, the atomic layer in a SWNT cannot be divided into different layers and the flexural strain or deformation are actually concentrated on a narrow region around the center-line of the atom layer, rather than distributed linearly over the thickness direction.

Hence it is inappropriate to assume straight normal postulate for CNTs. Hence Wang et al. (2005) proposed that since the representative thickness of the nanotube layer is 0.066 nm (Yakobson et al., 1996) which is much smaller than the diameter of the tube, the stiffness of the nanotube beam structure for a SWNT can be expressed as follows

$$EI = \frac{E\pi}{64}\left(d_o^4 - d_i^4\right) \tag{13}$$

Substituting the equality $d_o - d_i = 2h$ and $d_o \approx d_i \approx d$

$$EI = \frac{\pi Et}{8} d^3 = \frac{\pi C}{8} d^3 \tag{14}$$

Where d_o is the outer diameter, d_i is the inner diameter, $Et = C = 360 J/m^2$ is the in-plane stiffness of CNT.

3.2.3 Mass Density

Yoon et al., (2004) proposed $\rho = 1.3 g/cm^3$. The cross area of the nanotube is given by $A = \pi dt$. Since a SWNT is rolled up from a sheet of graphite, the value of thickness in calculating the cross area of the CNT should be used from the equilibrium interlayer spacing of adjacent nanotubes, i.e. $t = 0.34nm$, which is shown in figure VII.

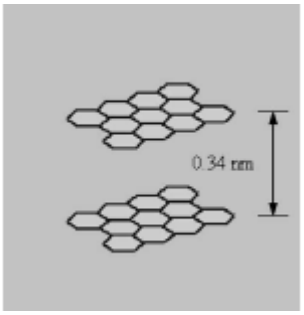

Figure VII Interlayer Spacing of Adjacent Nanotube

3.3 Continuum Models of CNTs

3.3.1 Continuum Model of Single Walled CNTs

Equation for SWNT is given by

$$EI\frac{\partial^4 w(x,t)}{\partial x^4}+\rho A\frac{\partial^2 w(x,t)}{\partial x^2}=0 \tag{15}$$

Substituting the bending stiffness proposed by Wang et al. (2004), where $EI=\frac{\pi C}{8}d^3$

$$\frac{\pi}{8}Cd^3\frac{\partial^4 w(x,t)}{\partial x^4}+\rho A\frac{\partial^2 w(x,t)}{\partial t^2}=0 \tag{16}$$

The free vibration solution can be found using the method of separation of variables

$$w(x,t)=W(x)T(t) \tag{17}$$

Substituting in the eq (17) in eq (16)

$$\frac{\pi}{8}Cd^3\frac{d^4W(x)}{dx^4}T(t)+\rho A\frac{d^2T(t)}{dt^2}W(x)=0 \tag{18}$$

$$\left[\frac{\pi}{8}\frac{Cd^3}{\rho A}\frac{d^4W(x)}{dx^4}\right]\frac{1}{W(x)}=\omega^2 \tag{19}$$

$$\frac{\pi}{8}\frac{Cd^3}{\rho A}\frac{d^4W(x)}{dx^4}-\omega^2W(x)=0 \tag{20}$$

By substituting $\frac{d^4W}{dx^4}-\beta^4W=0$; Where $\beta^4=\frac{\omega^2}{q^2}$ & $q^2=\frac{\pi Cd^3}{8\rho A}$ (21)

$$\frac{\pi}{8}\frac{Cd^3}{\rho A}\beta^4W(x)-\omega^2W(x)=0 \tag{22}$$

$$\omega^2=\beta^4\frac{\pi}{8}\frac{Cd^3}{\rho A} \tag{23}$$

Substituting Area, $A=\pi dt$ and $\overline{\beta}^2=(\beta L)^2$

$$\omega=\frac{\overline{\beta}^2}{L^2}\sqrt{\frac{\pi Cd^3}{8\pi d\rho t}} \tag{24}$$

The natural frequency for a SWNT is given by

$$\omega=\frac{\overline{\beta}^2}{L^2}\sqrt{\frac{Cd^2}{8\rho t}} \tag{25}$$

where $\overline{\beta}$ depends on end conditions and mode number. For fixed end conditions $\overline{\beta}$ is 4.730041, 7.853205, 10.995608, 14.137165 and 17.278 for first five mode shapes respectively.

For cantilever end conditions $\overline{\beta}$ is 1.875104, 4.730041, 7.853205, 10.995608 and 14.137165 for first five mode shapes respectively.

3.3.2 Continuum Model of Double Walled CNTs

Equations for vibration of double walled CNTs are

$$c_1(w_2 - w_1) = EI_1 \frac{\partial^4 w_1}{\partial x^4} + \rho A_1 \frac{\partial^2 w_1}{\partial t^2} \tag{26}$$

$$-c_1(w_2 - w_1) = EI_2 \frac{\partial^4 w_2}{\partial x^4} + \rho A_2 \frac{\partial^2 w_2}{\partial t^2} \tag{27}$$

Substituting the bending stiffness proposed by Wang et al. (2004), where $EI = \frac{\pi C}{8} d^3$

$$c_1(w_2 - w_1) = \frac{\pi}{8} C d_1^{\,3} \frac{\partial^4 w_1}{\partial x^4} + \rho A_1 \frac{\partial^2 w_1}{\partial t^2} \tag{28}$$

$$-c_1(w_2 - w_1) = \frac{\pi}{8} C d_2^{\,3} \frac{\partial^4 w_2}{\partial x^4} + \rho A_2 \frac{\partial^2 w_2}{\partial t^2} \tag{29}$$

The free vibration solution can be found using the method of separation of variables

$$w_I(x,t) = W_I(x)T(t) \tag{30}$$

Substituting in the eq (30) into eqs (28) & (29)

$$\frac{\pi}{8} C d_1^{\,3} \frac{d^4 W_1(x)}{dx^4} - c_1 \left[W_2(x) - W_1(x) \right] - \rho A_1 \omega^2 W_1(x) = 0 \tag{31}$$

$$\frac{\pi}{8} C d_2^{\,3} \frac{d^4 W_2(x)}{dx^4} + c_1 \left[W_2(x) - W_1(x) \right] - \rho A_2 \omega^2 W_2(x) = 0 \tag{32}$$

Assuming that all the nested tubes have the same vibration modes $W_i(x)$, determined by

$$\frac{d^4 W_i(x)}{dx^4} - \beta^4 W_i(x) = 0 \tag{33}$$

Assuming $W_1(x) = aW(x)$ (34)

$$W_2(x) = bW(x) \tag{35}$$

Substituting the eqs (33) to (35) in eq (31) and eq (32), we have an Eigen value problem

$$\left[\frac{\pi}{8} C d_1^{\,3} \beta^4 + c_1 - \rho A_1 \omega^2 \right] a - \left[c_1 \right] b = 0 \tag{36}$$

$$-\left[c_1 \right] a + \left[\frac{\pi}{8} C d_2^{\,3} \beta^4 + c_1 - \rho A_2 \omega^2 \right] b = 0 \tag{37}$$

For a non-trivial solutions of a and b, the determinant of their co-efficient must be zero.

$$\begin{vmatrix} \frac{\pi}{8} C d_1^{\,3} \beta^4 + c_{12} - \rho A_1 \omega^2 & -c_1 \\ -c_1 & \frac{\pi}{8} C d_2^{\,3} \beta^4 + c_1 - \rho A_2 \omega^2 \end{vmatrix} = 0 \tag{38}$$

Expanding the determinant gives the frequency equation

$$\omega^4 - \left(\frac{\pi C {d_1}^3 \overline{\beta}^4 + 8L^4 c_1}{8L^4 \rho \pi t d_1} + \frac{\pi C {d_2}^3 \overline{\beta}^4 + 8L^4 c_1}{8L^4 \rho \pi t d_2} \right) \omega^2 + \left(\frac{8L^4 C \overline{\beta}^4 c_1 ({d_1}^3 + {d_2}^3) + \pi C^2 {d_1}^3 {d_2}^3 \overline{\beta}^8}{64 \pi L^8 \rho^2 t^2 d_1 d_2} \right) = 0 \quad (39)$$

Let $$\xi = \frac{\pi C {d_1}^3 \overline{\beta}^4 + 8L^4 c_1}{8L^4 \rho \pi t d_1} + \frac{\pi C {d_2}^3 \overline{\beta}^4 + 8L^4 c_1}{8L^4 \rho \pi t d_2} \quad (39a)$$

$$\zeta = \frac{8L^4 C \overline{\beta}^4 c_1 ({d_1}^3 + {d_2}^3) + \pi C^2 {d_1}^3 {d_2}^3 \overline{\beta}^8}{64 \pi L^8 \rho^2 t^2 d_1 d_2} \quad (39b)$$

Substituting eq (39a) and eq (39b), eq (39) becomes

$$\omega^4 - \xi \omega^2 + \zeta = 0 \quad (40)$$

The frequencies are given by

$${\omega_{n0}}^2 = \frac{1}{2}(\xi - \sqrt{\xi^2 - 4\zeta}) \;\&\; {\omega_{n1}}^2 = \frac{1}{2}(\xi + \sqrt{\xi^2 - 4\zeta}) \quad (41)$$

3.3.3 Continuum Model of Five Walled CNTs

The governing equations for five walled carbon nanotube is given by

$$c_1(w_2-w_1) = EI_1 \frac{\partial^4 w_1}{\partial x^4} + \rho A_1 \frac{\partial^2 w_1}{\partial t^2} \tag{42}$$

$$c_2(w_3-w_2) - c_1(w_2-w_1) = EI_2 \frac{\partial^4 w_2}{\partial x^4} + \rho A_2 \frac{\partial^2 w_2}{\partial t^2} \tag{43}$$

$$c_3(w_4-w_3) - c_2(w_3-w_2) = EI_3 \frac{\partial^4 w_3}{\partial x^4} + \rho A_3 \frac{\partial^2 w_3}{\partial t^2} \tag{44}$$

$$c_4(w_5-w_4) - c_3(w_4-w_3) = EI_4 \frac{\partial^4 w_4}{\partial x^4} + \rho A_4 \frac{\partial^2 w_4}{\partial t^2} \tag{45}$$

$$-c_4(w_5-w_4) = EI_5 \frac{\partial^4 w_5}{\partial x^4} + \rho A_5 \frac{\partial^2 w_5}{\partial t^2} \tag{46}$$

Substituting the bending stiffness proposed by Wang et al. (2004), where $EI = \frac{\pi C}{8} d^3$

$$c_1(w_2-w_1) = \frac{\pi}{8} C d_1^{\,3} \frac{\partial^4 w_1}{\partial x^4} + \rho A_1 \frac{\partial^2 w_1}{\partial t^2} \tag{47}$$

$$c_2(w_3-w_2) - c_1(w_2-w_1) = \frac{\pi}{8} C d_2^{\,3} \frac{\partial^4 w_2}{\partial x^4} + \rho A_2 \frac{\partial^2 w_2}{\partial t^2} \tag{48}$$

$$c_3(w_4-w_3) - c_2(w_3-w_2) = \frac{\pi}{8} C d_3^{\,3} \frac{\partial^4 w_3}{\partial x^4} + \rho A_3 \frac{\partial^2 w_3}{\partial t^2} \tag{49}$$

$$c_4(w_5-w_4) - c_3(w_4-w_3) = \frac{\pi}{8} C d_4^{\,3} \frac{\partial^4 w_4}{\partial x^4} + \rho A_4 \frac{\partial^2 w_4}{\partial t^2} \tag{50}$$

$$-c_4(w_5-w_4)=\frac{\pi}{8}Cd_5{}^3\frac{\partial^4 w_5}{\partial x^4}+\rho A_5\frac{\partial^2 w_5}{\partial t^2} \tag{51}$$

The free vibration solution can be found using the method of separation of variables

$$w_I(x,t)=W_I(x)T(t) \tag{52}$$

Substituting in the eq (52) into eqs (47) to (51)

$$\frac{\pi}{8}Cd_1{}^3\frac{d^4W_1(x)}{dx^4}-c_1\left[W_2(x)-W_1(x)\right]-\rho A_1\omega^2W_1(x)=0 \tag{53}$$

$$\frac{\pi}{8}Cd_2{}^3\frac{d^4W_2(x)}{dx^4}-c_2\left[W_3(x)-W_2(x)\right]+c_1\left[W_2(x)-W_1(x)\right]-\rho A_2\omega^2W_2(x)=0 \tag{54}$$

$$\frac{\pi}{8}Cd_3{}^3\frac{d^4W_3(x)}{dx^4}-c_3\left[W_4(x)-W_3(x)\right]+c_2\left[W_3(x)-W_2(x)\right]-\rho A_3\omega^2W_3(x)=0 \tag{55}$$

$$\frac{\pi}{8}Cd_4{}^3\frac{d^4W_4(x)}{dx^4}-c_4\left[W_5(x)-W_4(x)\right]+c_3\left[W_4(x)-W_3(x)\right]-\rho A_4\omega^2W_4(x)=0 \tag{56}$$

$$\frac{\pi}{8}Cd_5{}^3\frac{d^4W_5(x)}{dx^4}+c_4\left[W_5(x)-W_4(x)\right]-\rho A_5\omega^2W_5(x)=0 \tag{57}$$

Assuming that all the nested tubes have the same vibration modes $W_i(x)$, determined by

$$\frac{d^4W_i(x)}{dx^4}-\beta^4W_i(x)=0 \tag{58}$$

Assuming $W_1(x)=aW(x)$ (59)

$W_2(x)=bW(x)$ (60)

$$W_3(x) = cW(x) \tag{61}$$

$$W_4(x) = dW(x) \tag{62}$$

$$W_5(x) = eW(x) \tag{63}$$

Substituting the eqs (58) to (63) in eqs (53) to (57), we have an Eigen value problem

$$\left[\frac{\pi}{8} C d_1^{\,3} \beta^4 + c_1 - \rho A_1 \omega^2\right] a - [c_1] b = 0 \tag{64}$$

$$-[c_1] a + \left[\frac{\pi}{8} C d_2^{\,3} \beta^4 + c_1 - \rho A_2 \omega^2\right] b - [c_2] c = 0 \tag{65}$$

$$-[c_2] b + \left[\frac{\pi}{8} C d_3^{\,3} \beta^4 + c_3 + c_2 - \rho A_3 \omega^2\right] c - [c_3] d = 0 \tag{66}$$

$$-[c_3] c + \left[\frac{\pi}{8} C d_4^{\,3} \beta^4 + c_4 + c_3 - \rho A_4 \omega^2\right] d - [c_4] e = 0 \tag{67}$$

$$-[c_4] d + \left[\frac{\pi}{8} C d_5^{\,3} \beta^4 + c_4 - \rho A_5 \omega^2\right] e = 0 \tag{68}$$

For a non-trivial solutions of a, b, c, d and e the determinant of their co-efficient must be zero. Expanding the determinant will give the frequency equation

$$\begin{vmatrix} \frac{\pi}{8} C d_1^3 \beta^4 + c_1 - \rho A_1 \omega^2 & -c_1 & 0 & 0 & 0 \\ -c_1 & \frac{\pi}{8} C d_2^3 \beta^4 + c_2 + c_1 - \rho A_2 \omega^2 & -c_2 & 0 & 0 \\ 0 & -c_2 & \frac{\pi}{8} C d_3^3 \beta^4 + c_3 + c_2 - \rho A_3 \omega^2 & -c_3 & 0 \\ 0 & 0 & -c_3 & \frac{\pi}{8} C d_4^3 \beta^4 + c_4 + c_3 - \rho A_4 \omega^2 & -c_4 \\ 0 & 0 & 0 & -c_4 & \frac{\pi}{8} C d_5^3 \beta^4 + c_4 - \rho A_5 \omega^2 \end{vmatrix} = 0 \tag{69}$$

CHAPTER 4 FINITE ELEMENT ANALYSIS

4.1 Introduction

The finite element method (FEM) has become a powerful numerical method for analyzing physical phenomena in the fields of structural, solid and fluid mechanics. In the last almost four decades, the finite element method (FEM) has become the prevalent technique used for analyzing physical phenomena in the field of structural, solid and fluid mechanics as well as for solution of field problems. The FEM is a useful tool because one can use it to find out facts or study the process in a way not possible with any other tool.

The computational approach is an important tool in the development of nano composites and their properties. It helps to understand and design these novel materials. By means of finite element method, it is possible to identify mechanical, thermal and electrical properties and to study their structural responses under various loads.

Finite element analysis enables to create parameters and boundary conditions, which are not accessible experimentally, or analytically to be investigated. Finite element analysis has three basic stages. They are Pre-Processing, Analysis, Post-Processing

Basically pre-processing involves discretization of domain of interest into finite elements. The elements are connected to each other through nodes. Discretization is one of the basic and

important steps in finite element analysis. The quality of output will depend upon the quality of the element and quality of meshing. The basic unknown parameter is the displacement at the nodal points. The next step is defining physical and material properties for the elements. All these steps come under meshing. Then loads and boundary conditions are applied.

The analysis stage involves stiffness generation, mass generation, stiffness modification and solution of equations resulting in the evaluation of nodal variables. Other derived quantities such as gradients or stresses may be evaluated at this stage. A stiffness and mass matrix are formed for all the elements and are assembled to obtain the global matrices. Then by applying the boundary conditions, the global matrices are modified and the displacements are calculated by solving the finite element equations, which in turn is used to calculate the stresses and strains. The post-processing stage is concerned with interrogating the results of the analysis. In case of free vibration this will be the natural frequencies and modes of free vibration.

Pre-processing for all FE models of SWNT and MWNT are done using finite element software I-DEAS. Preprocessing includes discretization of the structure, applying material and physical properties, applying loads and boundary conditions. Analysis and Post-processing, where done using powerful finite element software called ABAQUS.

4.2 Bulk Properties of Nanotube in FE Modeling

Material properties of CNTs should be chosen correctly to simulate the actual nano-effects. In continuum modeling, we use thickness (t) of 0.34 while calculating the area of the nanotube and thickness (t) of 0.066nm while calculating bending rigidity. The young's modulus used in continuum modeling is 5 Tpa. In finite element modeling we can't use two thicknesses so we have to use a constant thickness (t_s) of 0.34 nm. The young's modulus of nanotube is modified to 1 Tpa so that in-plane stiffness(C) of nanotube is maintained as 360 J/m^2. Since finite element codes cannot be directly applied to a nano-scale because of their smaller dimensions, so the nano-scale problem has to be scaled up for solving using finite element codes. The nano model is scaled to a model, which is in meter-scale.

4.3 Finite Element Modeling

4.3.1 FE Model of Single Walled CNT

The finite element modeling of single walled nanotube is easy since there is no van der Waals force. Abaqus Euler-Bernoulli beams B23 (2 noded cubic beam) shown in figure VIII were used to model single walled nanotube.

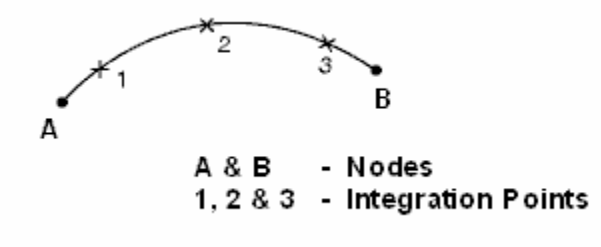

Figure VIII B23 Beam Element

This beam element is a one-dimensional line element that has stiffness associated with deformation of the line (Beam's axis). These deformations consist of axial stretch; curvature change (Bending) and torsion. This element does not allow transverse shear deformation; plane section initially normal to the beam's axis remains plane and normal to the beam axis. The Euler-Bernoulli beam elements use cubic interpolation functions. The main advantage of this element is that they are geometrically simple, few degrees of freedom and computational time is less.

First step in finite element model of SWNT is to create a set of 20 nodes. Then Abaqus pipe section is selected as the beam cross-section.

Second step is creating 19 beam elements between the nodes. The third step is to assign appropriate material properties to the elements. The fourth step is fixing the left most node of the beam so that it simulates cantilever boundary condition. The fifth step is to select Lanzcos Eigen value extraction method. The sixth step is to solve for Eigen values. The final step is to post process the results obtained. Figure IX shows the finite element model of SWNT.

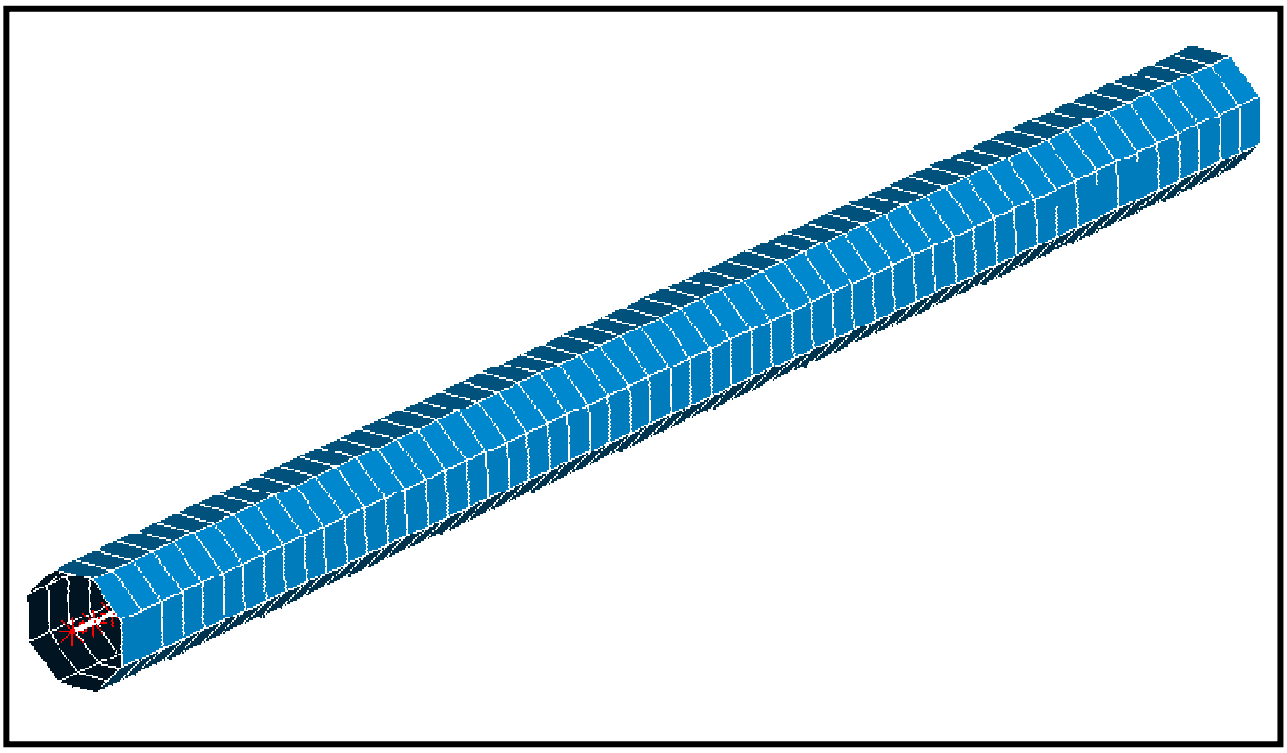

Figure IX Finite Element Model of SWNT

4.3.2 FE Model of Double Walled CNT

For double walled nanotube, 8 noded linear solid brick elements shown in figure X were used for modeling the two tubes.

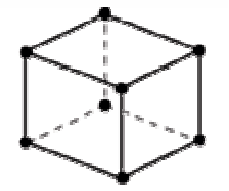

Figure X C3D8 – Linear Brick Element

From structural mechanics viewpoint, the effect of van der Waals force is like a distributed spring with stiffness C_N attached at the interface of inner and outer tube. A special spring element called axial spring element are used to simulate the effect of van der Waals force. Figure XI shows the axial spring element. This special spring element's line of action is the line joining the two nodes. This spring element introduces stiffness between two degrees of freedom without introducing an associated mass.

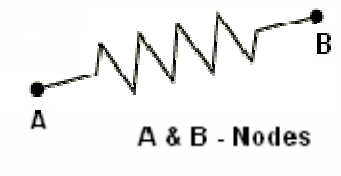

Figure XI Axial Spring Element

First a quarter of the model is modeled and then it is reflected to make the complete model, by this way the model is symmetric. Once the model is reflected, then the procedure is same as SWNT. Appropriate material properties and boundary conditions are applied and then the model is solved for natural frequencies. Figure XII shows the finite element model of SWNT.

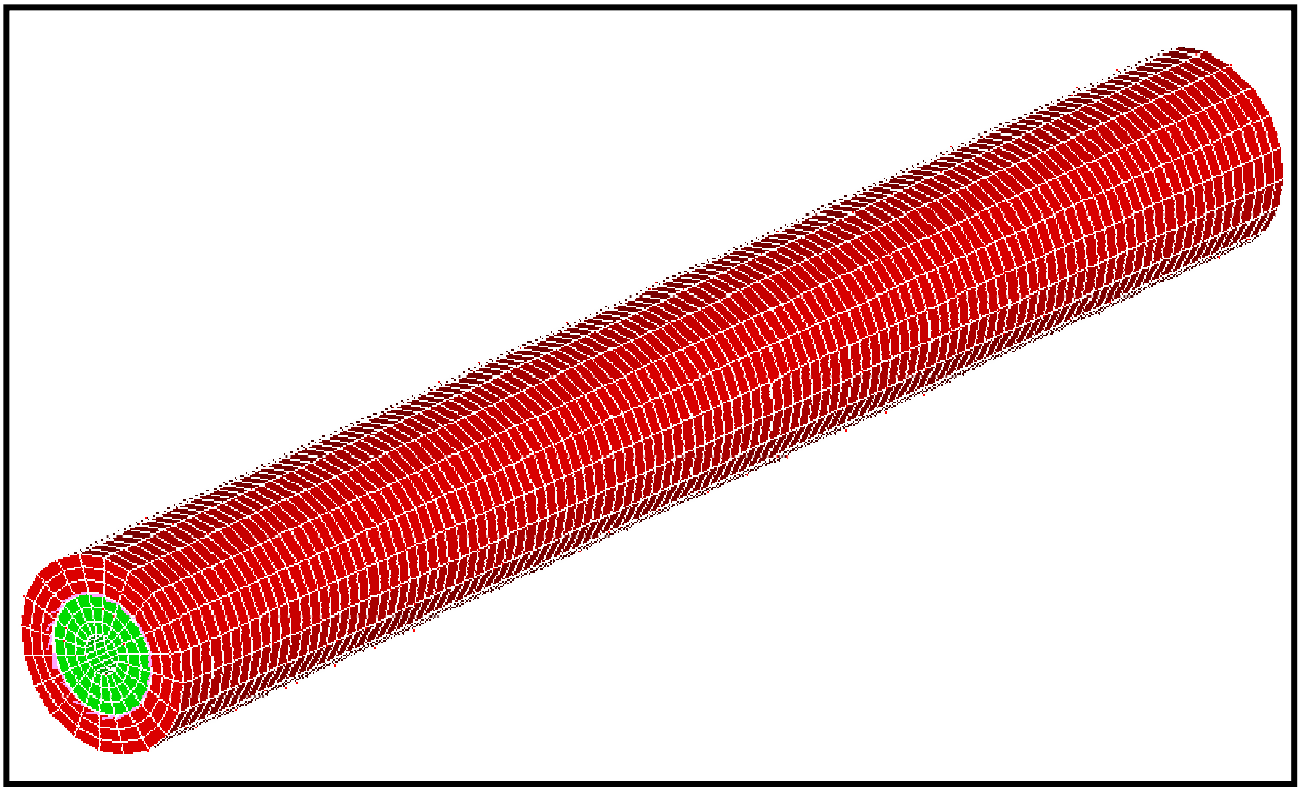

Figure XII Finite Element Model of DWNT

4.3.3 FE Model of Five Walled CNT

For multi walled nanotube, 8 noded solid brick elements were used for modeling the individual tubes of MWNT (modeling is similar to DWNT). Axial spring elements are used to simulate the effect of van der Waals force. First a quarter of the model is modeled and then it is reflected to make the complete model. Once the model is reflected, then the procedure is same as DWNT. Appropriate material properties and boundary conditions are applied and then the model is solved for natural frequencies. Figure XIII shows the finite element model of five walled nanotube

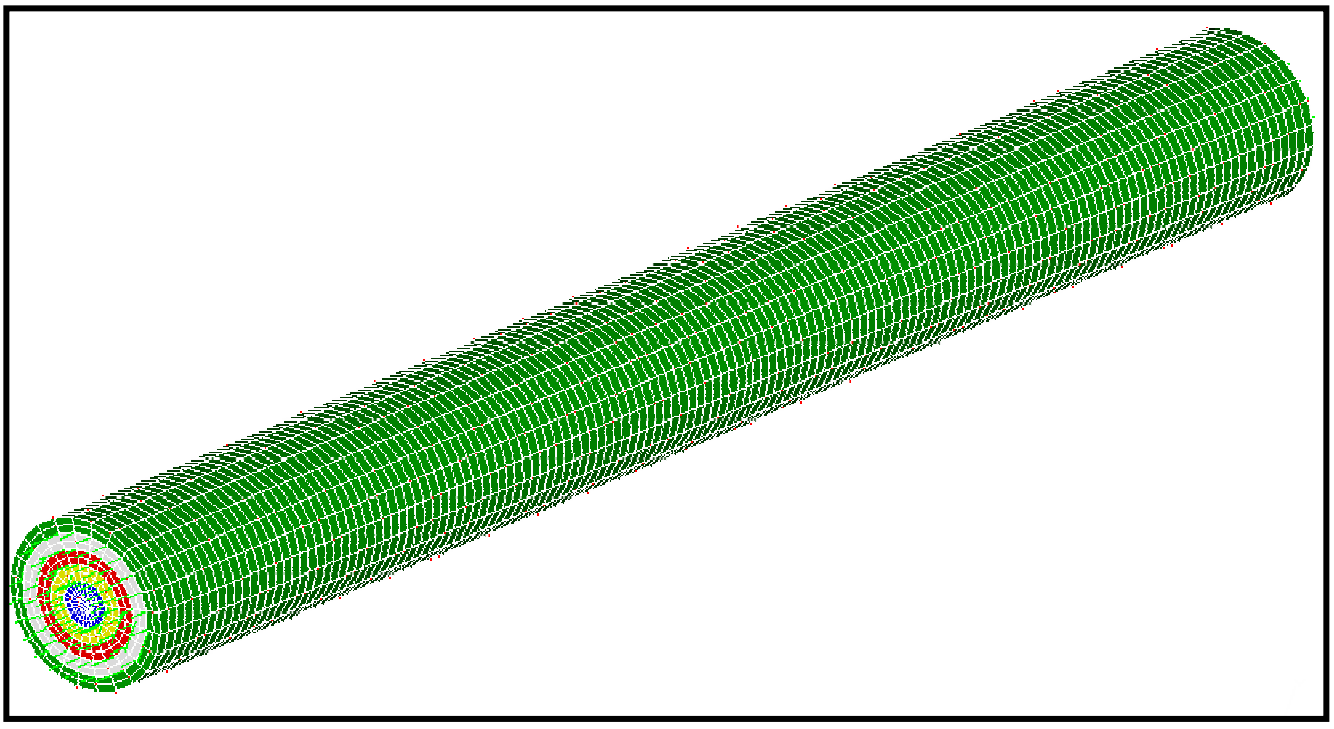

Figure XIII Finite Element Model of Five Walled Nanotube

Figure XIV shows finite element models for single, double and five-walled nanotube. It also shows the axial spring between inner and outer tube of double walled nanotube

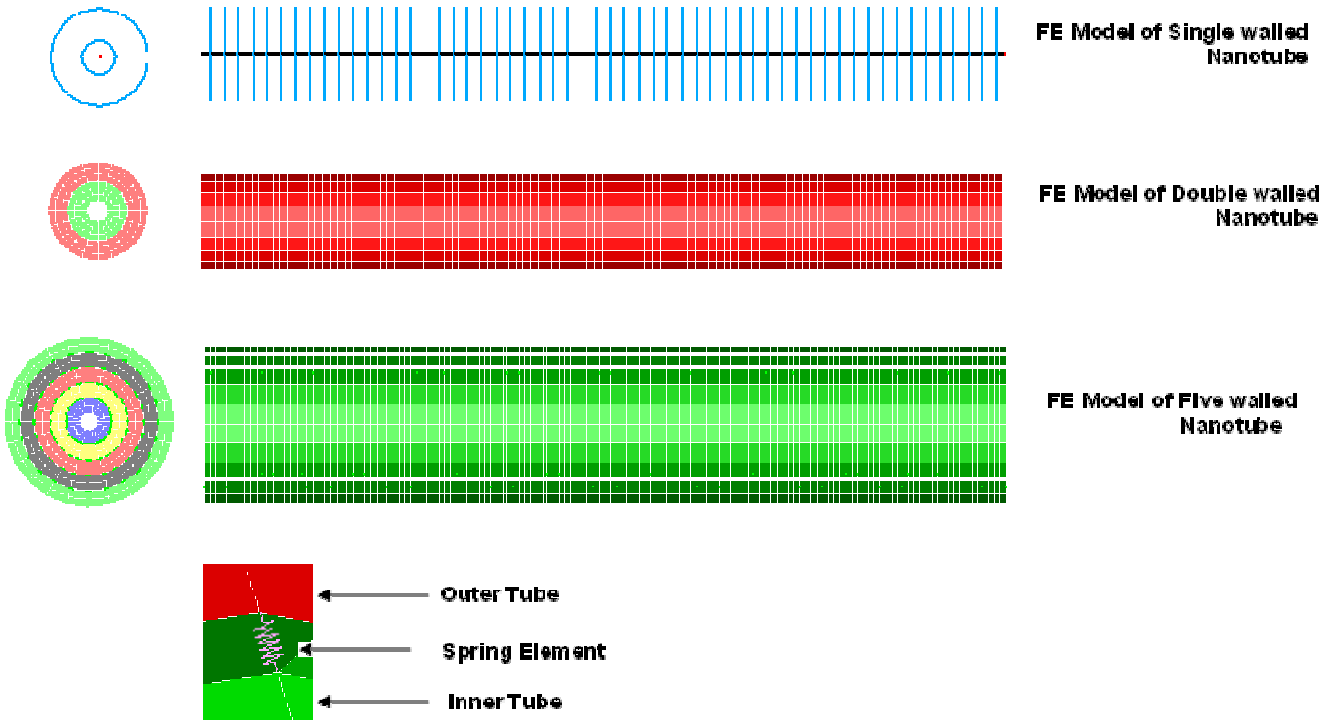

Figure XIV FE models for Single and Multi walled nanotubes

.

4.4 Eigen Value Extraction

The Eigen value problem for the natural frequencies of an undamped finite element model is given by

$$\left(-\omega^2 M^{xy} + K^{xy}\right)\phi^x = 0 \qquad (70)$$

M^{xy} - Mass Matrix

K^{xy} - Stiffness Matrix

ϕ^x - Eigen Vector (Mode of Vibration)

ω - Frequency

x and y – Degrees of freedom

ABAQUS offers two methods for eigenvalue extraction. They are Lanczos and subspace eigenvalue extraction methods. I have used Lanczos method because it is generally faster when a large number of eigenmodes is required for a system with many degrees of freedom.

4.5 Frequency Calculation

4.5.1 Frequency of Single walled CNT

The frequencies obtained using finite element model has to be scaled down using scaling factors to get the natural frequencies of the nano-size problem.

Frequency of actual model, $$\omega = \frac{\overline{\beta}^2}{L^2}\sqrt{\frac{Cd^2}{8\rho t}} \tag{71}$$

Frequency of scaled Model $$\omega_s = \frac{\overline{\beta}^2}{{L_s}^2}\sqrt{\frac{E_s I_s}{\rho_s A_s}} \tag{72}$$

Where ω is the frequency, d is the diameter, ρ is the density, L is the length of single walled nanotube (actual model). ω_s is the frequency, ρ_s is the density, L_s is the length, A_s is area, E_s is the young's modulus, I_s is the moment of inertia of scaled (finite element) model.

Ratio of frequencies of actual and scaled model is given by

$$\frac{\omega}{\omega_s} = \frac{\frac{\overline{\beta}^2}{L^2}\sqrt{\frac{Cd^2}{8\rho t}}}{\frac{\overline{\beta}^2}{{L_s}^2}\sqrt{\frac{E_s I_s}{\rho_s A_s}}} \tag{73}$$

Frequencies of actual model in terms of scaled model is given by

$$\omega = \omega_s * \frac{{L_s}^2}{L^2} * \sqrt{\frac{EI}{E_s I_s}} * \sqrt{\frac{\rho_s}{\rho}} * \sqrt{\frac{A_s}{A}} \tag{74}$$

4.5.2 Frequency of Double walled CNT

Frequency of actual model is given by

$$\omega_{n0}{}^2 = \frac{1}{2}(\xi - \sqrt{\xi^2 - 4\zeta}) \quad \& \quad \omega_{n1}{}^2 = \frac{1}{2}(\xi + \sqrt{\xi^2 - 4\zeta}) \tag{75a}$$

where $$\xi = \frac{\pi C d_1{}^3 \overline{\beta}^4 + 8L^4 c_1}{8L^4 \rho \pi t d_1} + \frac{\pi C d_2{}^3 \overline{\beta}^4 + 8L^4 c_1}{8L^4 \rho \pi t d_2} \tag{75b}$$

$$\zeta = \frac{8L^4 C \overline{\beta}^4 c_1 (d_1{}^3 + d_2{}^3) + \pi C^2 d_1{}^3 d_2{}^3 \overline{\beta}^8}{64\pi L^8 \rho^2 t^2 d_1 d_2} \tag{75c}$$

where ω_{n0} and ω_{n1} are the frequencies , d_1 and d_2 are the diameter of inner and outer tubes , C is the in-plane stiffness, L is the length, ρ is the mass density , c_1 is the van der Waals force between inner and outer tubes of the DWNT (actual model).

Frequency of scaled model is given by

$$(\omega_{n0})_s{}^2 = \frac{1}{2}(\xi_s - \sqrt{\xi_s{}^2 - 4\zeta_s}) \quad \& \quad (\omega_{n1})_s{}^2 = \frac{1}{2}(\xi_s + \sqrt{\xi_s{}^2 - 4\zeta_s}) \tag{76a}$$

where $$\xi_s = \frac{E_s I_{1s} \beta^4 + c_{1s}}{\rho_s A_{1s}} + \frac{E I_{s2} \beta^4 + c_{1s}}{\rho_s A_{2s}} \tag{76b}$$

$$\zeta_s = \frac{E_s I_{1s} \beta^4 c_{1s} + E_s I_{2s} \beta^4 c_{1s}}{\rho_s A_{1s} \rho_s A_{2s}} + \frac{E_s I_{1s} E_s I_{2s} \beta^8}{\rho_s A_{1s} \rho_s A_{2s}} \tag{76c}$$

where $(\omega_{n0})_s$ and $(\omega_{n1})_s$ are the frequencies, E_s is the young's modulus , ρ_s is the mass density, I_{1s} is the moment of inertia of , A_{1s} and A_{2s} are the area of the cross-section of inner and outer tubes, c_{1s} is the van der Waals force between inner and outer tubes of scaled DWNT (finite element model).

Ratio of frequencies of actual and scaled model is given by

$$\frac{{\omega_{n0}}^2}{{(\omega_{n0})_s}^2} = \frac{\frac{1}{2}(\xi - \sqrt{\xi^2 - 4\zeta})}{\frac{1}{2}(\xi_s - \sqrt{{\xi_s}^2 - 4\zeta_s})} \quad \& \quad \frac{{\omega_{n1}}^2}{{(\omega_{n1})_s}^2} = \frac{\frac{1}{2}(\xi + \sqrt{\xi^2 - 4\zeta})}{\frac{1}{2}(\xi_s + \sqrt{{\xi_s}^2 - 4\zeta_s})} \tag{77}$$

Frequencies of actual model in terms of scaled model is given by

$${\omega_{n0}}^2 = {(\omega_{n0})_s}^2 * \frac{(\xi - \sqrt{\xi^2 - 4\zeta})}{(\xi_s - \sqrt{{\xi_s}^2 - 4\zeta_s})} \quad \& \quad {\omega_{n1}}^2 = {(\omega_{n1})_s}^2 * \frac{(\xi + \sqrt{\xi^2 - 4\zeta})}{(\xi_s + \sqrt{{\xi_s}^2 - 4\zeta_s})} \tag{78}$$

CHAPTER 5 RESULTS AND DISCUSSION

5.1 Continuum Model Results

Table I Frequencies of fixed DWNT (with inner diameter 0.7nm, outer diameter 1.4nm and c_1=1e20 N/m^2)

Cases	Modes		Continuum Model (THz)	Single Beam Theory (THz)	% of Error
L/d_2=10	1	ω11	1.39	1.39	0.00
	2	ω21	3.84	3.84	0.00
	3	ω31	7.54	7.54	0.00
	4	ω41	12.47	12.47	0.00
	5	ω51	18.63	18.63	0.00
L/d_2=20	1	ω11	0.35	0.35	0.00
	2	ω21	0.96	0.96	0.00
	3	ω31	1.88	1.88	0.00
	4	ω41	3.11	3.11	0.00
	5	ω51	4.65	4.65	0.00
L/d_2=50	1	ω11	0.06	0.06	0.00
	2	ω21	0.15	0.15	0.00
	3	ω31	0.30	0.30	0.00
	4	ω41	0.49	0.49	0.00
	5	ω51	0.75	0.75	0.00

If the value of c_1 is large, it can be verified that the effect of van der Waals force on MWNT is negligible and thus lower order frequency given by eq (41) will be equal to the frequency of single elastic beam model given by

$$\omega = \frac{\overline{\beta}^2}{L^2}\sqrt{\frac{\pi}{8}\frac{C(d_1^{\,3} + d_2^{\,3})}{\rho(A_1 + A_2)}} \tag{79}$$

Table I shows the natural frequencies of fixed double walled nanotube and an equivalent single beam. Fixed double walled CNTs should behave as a fixed single beam when the vanderwaals

force is very large (1e20 N/m^2). From table I, it is clear that the proposed continuum model for a fixed double walled nanotube is valid, since the percentage of error is zero.

Table II Frequencies of fixed DWNT (with inner diameter 0.7nm and outer diameter 1.4nm)

Cases	Modes		Continuum Model (THz)	J. Yoon[9] (THz)	% of Error
$L/d_2=10$	1	ω_{11}	1.39	1.4	-0.71
		ω_{12}	10.62	10.3	3.10
	2	ω_{21}	3.79	3.8	-0.26
		ω_{22}	11.03	10.7	3.08
	3	ω_{31}	7.05	7.2	-2.08
		ω_{32}	12.52	12.3	1.78
	4	ω_{41}	10.31	10.6	-2.73
		ω_{42}	16.27	16.2	0.43
	5	ω_{51}	13.46	14.1	-4.53
		ω_{52}	22.55	22.5	0.22
$L/d_2=20$	1	ω_{11}	0.35	0.35	0.00
		ω_{12}	10.56	10.2	3.52
	2	ω_{21}	0.96	1.0	-4.00
		ω_{22}	10.59	10.2	3.82
	3	ω_{31}	1.88	1.9	-1.05
		ω_{32}	10.67	10.3	3.59
	4	ω_{41}	3.27	3.1	5.48
		ω_{42}	10.87	10.5	3.52
	5	ω_{51}	4.55	4.6	-1.08
		ω_{52}	11.27	11.0	2.45
$L/d_2=50$	1	ω_{11}	0.06	0.06	0.00
		ω_{12}	10.56	10.2	3.52
	2	ω_{21}	0.15	0.16	-6.25
		ω_{22}	10.56	10.2	3.52
	3	ω_{31}	0.30	0.31	-3.22
		ω_{32}	10.56	10.2	3.52
	4	ω_{41}	0.50	0.51	-2.15
		ω_{42}	10.57	10.2	3.62
	5	ω_{51}	0.75	0.75	0.00
		ω_{52}	10.58	10.2	3.72

Table III Frequencies of fixed DWNT (with inner diameter 0.7nm and outer diameter 1.4nm)

Cases	Modes		Continuum Model (THz)	Single Beam Theory (THz)	% of Error
L/d_2=10	1	ω_{11}	1.39	1.39	0.00
	2	ω_{21}	3.79	3.84	-1.30
	3	ω_{31}	7.05	7.54	-6.49
	4	ω_{41}	10.31	12.47	-17.3
	5	ω_{51}	13.46	18.63	-27.7
L/d_2=20	1	ω_{11}	0.35	0.35	0.00
	2	ω_{21}	0.96	0.96	0.00
	3	ω_{31}	1.88	1.88	0.00
	4	ω_{41}	3.27	3.11	5.14
	5	ω_{51}	4.55	4.65	-2.15
L/d_2=50	1	ω_{11}	0.06	0.06	0.00
	2	ω_{21}	0.15	0.15	0.00
	3	ω_{31}	0.30	0.30	0.00
	4	ω_{41}	0.50	0.49	2.04
	5	ω_{51}	0.75	0.75	0.00

Table IV Frequencies of cantilever DWNT (with inner diameter 0.7nm, outer diameter 1.4nm and c_1=1e20 N/m^2)

Cases	Modes		Continuum Model (THz)	Single Beam Theory (THz)	% of Error
L/d_2=10	1	ω_{11}	0.22	0.22	0.00
	2	ω_{21}	1.38	1.38	0.00
	3	ω_{31}	3.85	3.85	0.00
	4	ω_{41}	7.54	7.54	0.00
	5	ω_{51}	12.47	12.47	0.00
L/d_2=20	1	ω_{11}	0.06	0.06	0.00
	2	ω_{21}	0.34	0.34	0.00
	3	ω_{31}	0.96	0.96	0.00
	4	ω_{41}	1.89	1.89	0.00
	5	ω_{51}	3.11	3.11	0.00
L/d_2=50	1	ω_{11}	0.01	0.01	0.00
	2	ω_{21}	0.06	0.06	0.00
	3	ω_{31}	0.15	0.15	0.00
	4	ω_{41}	0.30	0.30	0.00
	5	ω_{51}	0.50	0.50	0.00

Table IV shows the natural frequencies of cantilevered double walled nanotube and an equivalent single beam. Cantilevered double walled CNTs should behave as an equivalent cantilevered single elastic beam model when the vanderwaals force is very large (1e20 N/m2). Since the percentage of error is zero it proves that the proposed continuum model for a fixed DWNT is valid.

Table V Frequencies of cantilever DWNT (with inner diameter 0.7nm and outer diameter 1.4nm)

Cases	Modes		Continuum Model (THz)	J. Yoon[9] (THz)	% of Error
$L/d_2=10$	1	ω_{11}	0.21	0.2	5.00
		ω_{12}	10.56	10.2	3.52
	2	ω_{21}	1.37	1.4	-2.14
		ω_{22}	10.62	10.3	3.10
	3	ω_{31}	3.79	3.8	-0.26
		ω_{32}	11.03	10.7	3.08
	4	ω_{41}	7.05	7.2	-2.08
		ω_{42}	12.51	12.3	1.70
	5	ω_{51}	10.31	10.6	-2.73
		ω_{52}	16.26	16.2	0.37
$L/d_2=20$	1	ω_{11}	0.06	0.06	0.00
		ω_{12}	10.56	10.2	3.52
	2	ω_{21}	0.34	0.35	-2.85
		ω_{22}	10.56	10.2	3.52
	3	ω_{31}	0.96	1.0	-4.00
		ω_{32}	10.59	10.2	3.82
	4	ω_{41}	1.89	1.9	-0.52
		ω_{42}	10.67	10.3	3.59
	5	ω_{51}	3.08	3.1	-0.64
		ω_{52}	10.87	10.5	3.52
$L/d_2=50$	1	ω_{11}	0.01	.01	0.00
		ω_{12}	10.56	10.2	3.52
	2	ω_{21}	0.06	0.06	0.00
		ω_{22}	10.56	10.2	3.52
	3	ω_{31}	0.15	0.16	-6.25
		ω_{32}	10.56	10.2	3.52
	4	ω_{41}	0.30	0.31	-3.22
		ω_{42}	10.56	10.2	3.52
	5	ω_{51}	0.50	0.51	-1.96
		ω_{52}	10.56	10.2	3.52

Table VI Frequencies of cantilever DWNT (with inner diameter 0.7nm and outer diameter 1.4nm)

Cases	Modes		Continuum Model (THz)	Single Beam Theory (THz)	% of Error
$L/d_2=10$	1	ω_{11}	0.21	0.22	-4.54
	2	ω_{21}	1.37	1.38	-0.72
	3	ω_{31}	3.79	3.85	-1.55
	4	ω_{41}	7.05	7.54	-6.49
	5	ω_{51}	10.31	12.47	-17.3
$L/d_2=20$	1	ω_{11}	0.06	0.06	0.00
	2	ω_{21}	0.34	0.34	0.00
	3	ω_{31}	0.96	0.96	0.00
	4	ω_{41}	1.89	1.89	0.00
	5	ω_{51}	3.08	3.11	-0.96
$L/d_2=50$	1	ω_{11}	0.01	0.01	0.00
	2	ω_{21}	0.06	0.06	0.00
	3	ω_{31}	0.15	0.15	0.00
	4	ω_{41}	0.30	0.30	0.00
	5	ω_{51}	0.50	0.50	0.00

It is seen from tables II, III, V and VI that the lowest intertube frequencies are almost same for fixed DWNT's and cantilever DWNT's indicating that they are insensitive to the end conditions as predicted by Yoon et al. (2002). The first three intertube frequencies are around 10 THz as predicted by Yoon et al. (2002). The intertube resonant frequency (ω_{n1}) is insensitive to the mode number and is much higher than the lowest natural frequency (ω_{n0}) for larger aspect ratios as predicted by Yoon et al. (2002). The percentage of error between continuum model and Yoon et al. (2002) and for lowest natural frequency (ω_{n0}) is almost negligible. But for cases $L/d_2>10$ the intertube frequency (ω_{n1}) is higher than the frequency calculated by Yoon et al. (2002) for both fixed and cantilever cases.

The continuum model is also compared with single beam theory. The frequency of single beam theory is given by

$$\omega = \frac{\overline{\beta}^2}{L^2}\sqrt{\frac{\frac{\pi}{8}C(d_1{}^3 + d_2{}^3)}{\rho(A_1 + A_2)}} \tag{80}$$

The difference between frequencies of continuum model and single beam theory can be seen from the tables III and VI. The difference clearly shows the effect of van der Waals force on vibration of nanotube. There is no effect of van der Waals force on vibration if $L/d_2>=50$. The highest effect of van der Waals force on vibration is 27 % for the fifth mode of fixed DWNT ($L/d_2=10$). The effect of van der Waals force is high for smaller aspect ratios ($L/d_2<=10$) and this effect decreases as the aspect ratio increases.

Table VII Frequencies of fixed five walled nanotube (with inner diameter 0.7 nm, outer diameter 3.5 nm and $L/d_5 = 10$)

Cases	Modes		Continuum Model (THz)	J. Yoon[9] (THz)	% of Error
$L/d_5 = 10$	1	ω_{11}	0.49	0.49	0.00
		ω_{12}	5.45	5.30	2.83
		ω_{13}	9.36	9.00	4.00
		ω_{14}	12.5	12.2	2.45
		ω_{15}	14.9	14.5	2.75
	2	ω_{11}	1.36	1.34	1.49
		ω_{12}	5.54	5.40	2.59
		ω_{13}	9.41	9.10	3.40
		ω_{14}	12.6	12.2	3.27
		ω_{15}	15.0	14.5	3.44
	3	ω_{11}	2.59	2.55	1.56
		ω_{12}	5.87	5.70	2.98
		ω_{13}	9.59	9.30	3.11
		ω_{14}	12.7	12.3	3.25
		ω_{15}	15.1	14.7	2.72
	4	ω_{11}	3.96	3.89	1.79
		ω_{12}	6.70	6.50	3.07
		ω_{13}	10.0	9.70	3.09
		ω_{14}	13.0	12.7	2.36
		ω_{15}	15.5	15.0	3.33
	5	ω_{11}	5.14	5.05	1.78
		ω_{12}	8.24	8.00	3.00
		ω_{13}	10.8	10.6	1.88
		ω_{14}	13.6	13.3	2.25
		ω_{15}	16.1	15.7	2.54

Table VIII Frequencies of fixed five walled nanotube (with inner diameter 0.7 nm, outer diameter 3.5 nm and $L/d_5 = 20$)

Cases	Modes		Continuum Model (THz)	J. Yoon[9] (THz)	% of Error
$L/d_5 = 20$	1	ω_{11}	0.12	0.12	0.00
		ω_{12}	5.43	5.30	2.45
		ω_{13}	9.35	9.00	3.88
		ω_{14}	12.5	12.1	3.30
		ω_{15}	14.9	14.5	2.75
	2	ω_{11}	0.34	0.34	0.00
		ω_{12}	5.44	5.30	2.64
		ω_{13}	9.35	9.00	3.88
		ω_{14}	12.5	12.1	3.30
		ω_{15}	14.9	14.5	2.75
	3	ω_{11}	0.67	0.66	1.51
		ω_{12}	5.46	5.30	3.01
		ω_{13}	9.36	9.10	2.85
		ω_{14}	12.5	12.2	2.45
		ω_{15}	14.9	14.5	2.75
	4	ω_{11}	1.10	1.09	0.91
		ω_{12}	5.51	5.30	3.96
		ω_{13}	9.39	9.10	3.18
		ω_{14}	12.5	12.2	2.45
		ω_{15}	15.0	14.5	3.44
	5	ω_{11}	1.64	1.61	1.86
		ω_{12}	5.60	5.40	3.70
		ω_{13}	9.44	9.10	3.73
		ω_{14}	12.6	12.2	3.27
		ω_{15}	15.0	14.5	3.44

Table IX Frequencies of fixed five walled nanotube (with inner diameter 0.7 nm, outer diameter 3.5 nm and $L/d_5 = 50$)

Cases	Modes		Continuum Model (THz)	J. Yoon[9] (THz)	% of Error
$L/d_5 = 50$	1	ω_{11}	0.02	0.02	0.00
		ω_{12}	5.43	5.30	2.45
		ω_{13}	9.35	9.00	3.88
		ω_{14}	12.5	12.1	3.30
		ω_{15}	14.9	14.5	2.75
	2	ω_{11}	0.05	0.05	0.00
		ω_{12}	5.43	5.30	2.45
		ω_{13}	9.35	9.00	3.88
		ω_{14}	12.5	12.1	3.30
		ω_{15}	14.9	14.5	2.75
	3	ω_{11}	0.11	0.11	0.00
		ω_{12}	5.43	5.30	2.45
		ω_{13}	9.35	9.00	3.88
		ω_{14}	12.5	12.1	3.30
		ω_{15}	14.9	14.5	2.75
	4	ω_{11}	0.17	0.18	-5.55
		ω_{12}	5.43	5.30	2.45
		ω_{13}	9.35	9.00	3.88
		ω_{14}	12.5	12.1	3.30
		ω_{15}	14.9	14.5	2.75
	5	ω_{11}	0.26	0.26	0.00
		ω_{12}	5.44	5.30	2.64
		ω_{13}	9.35	9.00	3.88
		ω_{14}	12.5	12.1	3.30
		ω_{15}	14.9	14.5	2.75

Table X Frequencies of fixed five walled nanotube (with inner diameter 0.7 nm and the outer diameter 3.5 nm)

Cases	Modes		Continuum Model (THz)	Single Beam Theory (THz)	% of Error
L/d_5=10	1	ω_{11}	0.49	0.59	-16.9
	2	ω_{21}	1.36	1.62	-16.0
	3	ω_{31}	2.59	3.19	-18.8
	4	ω_{41}	3.96	5.28	-25.0
	5	ω_{51}	5.14	7.88	-34.7
L/d_5=20	1	ω_{11}	0.12	0.14	-14.2
	2	ω_{21}	0.34	0.40	-15.0
	3	ω_{31}	0.67	0.79	-15.1
	4	ω_{41}	1.10	1.32	-16.6
	5	ω_{51}	1.64	1.97	-16.7
L/d_5=50	1	ω_{11}	0.02	0.02	0.00
	2	ω_{21}	0.05	0.06	-16.6
	3	ω_{31}	0.11	0.12	-8.33
	4	ω_{41}	0.17	0.21	-19.0
	5	ω_{51}	0.26	0.31	-16.1

Tables VII, VIII and IX show the frequency of fixed five walled CNTs with aspect ratios of 10, 20 and 50 respectively. From tables VII to IX it can be seen that the frequency of proposed continuum model is in agreement with the frequencies of Yoon et al. (2002). The percentage of error between these two models is almost negligible for the case L/d_5=50. Table X shows the frequencies of fixed five walled nanotube and fixed equivalent single beam. The percentage of difference between frequencies of continuum model and single beam is very large for the case L/d_5=10, which is 34% for the fifth mode. This effect decreases as the aspect ratio increases.

5.2 Finite Element Model Results

Table XI Frequency of cantilever SWNT

Length (nm)	Diameter (nm)	FE Model Frequency (THz)	Krishnan[4]-Method-I (THz)	% of Error
36.8	1.50	0.0391	0.0432	-9.49
24.3	1.52	0.0908	0.1040	-12.69
23.4	1.12	0.0722	0.0612	17.97

Table XII Frequency of cantilever SWNT

Length (nm)	Diameter (nm)	FE Model Frequency (THz)	Krishnan[4]-Method-II (THz)	% of Error
36.8	1.50	0.0391	0.0451	-13.30
24.3	1.52	0.0908	0.0996	-8.83
23.4	1.12	0.0722	0.0744	-2.95

Table XIII Frequency of cantilever SWNT

Length (nm)	Diameter (nm)	FE Model Frequency (THz)	Wang (THz)	% of Error
36.8	1.50	0.0391	0.0394	-0.76
24.3	1.52	0.0908	0.0913	-0.54
23.4	1.12	0.0722	0.0726	-0.55

Table XIV Frequencies of cantilever SWNT (diameter = 1.50 nm and length = 36.8 nm)

Mode	FE Model Frequency (THz)
1	0.0392
2	0.2462
3	0.6895
4	1.3512
5	2.2336

The validation of the proposed FE model for SWNT is done by comparing the results with Krishnan et al. (1998) and Wang et al. (2005) and for DWNT and MWNT is done by comparing the results with Yoon et al. (2002). Tables XI to XIII shows the comparison of finite element results of cantilever SWNT with the experimental results (Method – I & II) of Krishnan et al. (1998) and analytical results of Wang et al. (2005). The maximum percentage of error when compared with experimental results (Method – I) of Krishnan et al. (1998) is 17 %. The maximum and minimum percentage of error when compared with experimental results (Method – II) of Krishnan et al. (1998) is 13 % and 2 %. The maximum percentage of error when compared with analytical results of Wang et al. (2005) is 0.55 %. Hence the suggested finite element model for SWNT closely agrees with continuum model of Wang et al. (2005). Figure XV shows the first five mode shapes of cantilever SWNT predicted by proposed FE model. The mode shapes are similar to the mode shapes of any cantilever beam.

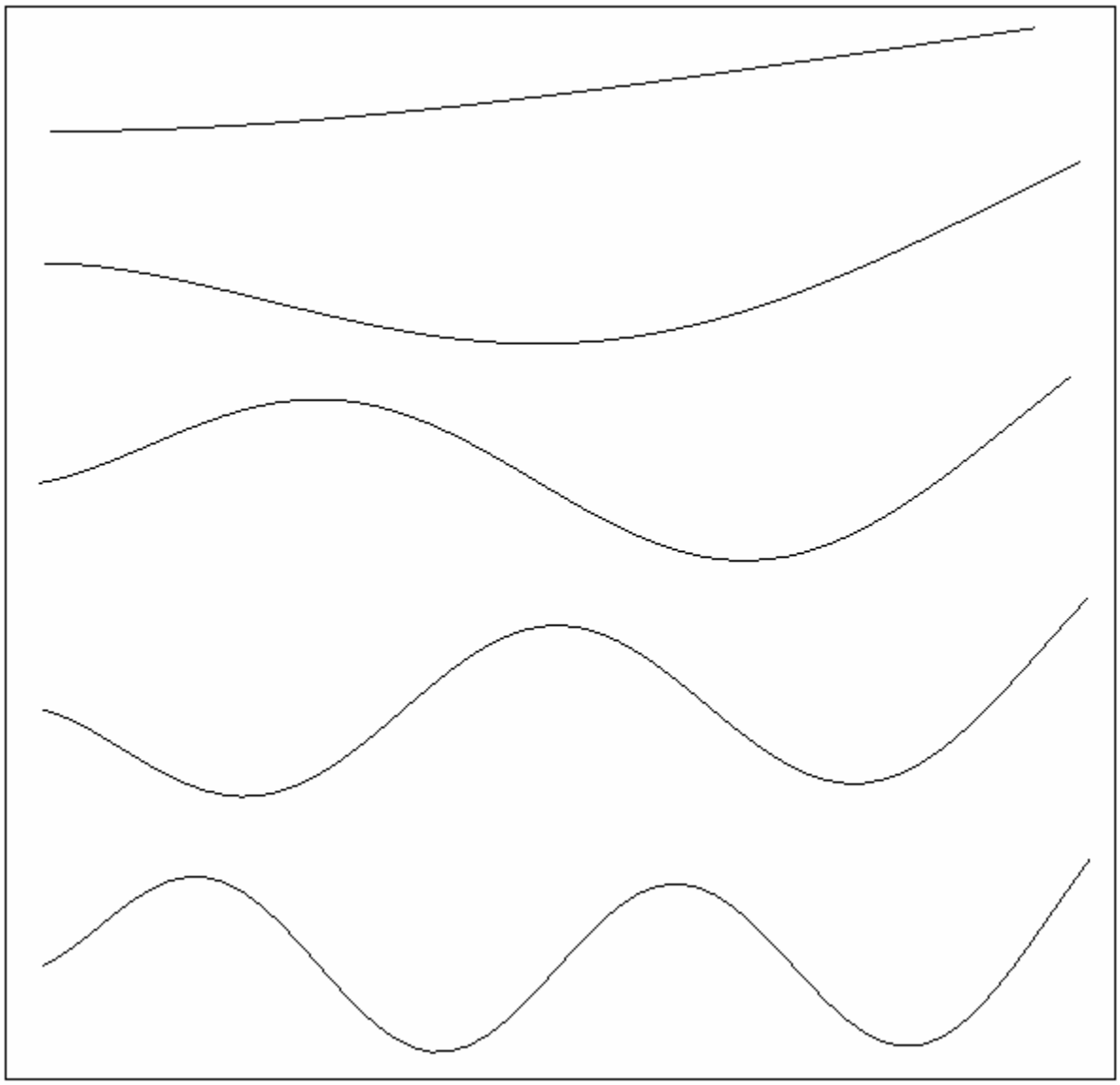

Figure XV First five modes of cantilevered SWNT (diameter=1.50 nm and length = 36.8 nm)

Table XV Frequencies of fixed DWNT (with inner diameter 0.7 nm. and the outer diameter 1.4 nm)

Cases	Modes		FE Model Frequency (THz)	J. Yoon[9] (THz)	% of Error
$L/d_2=10$	1	ω_{11}	1.39	1.4	-0.71
		ω_{12}	9.95	10.3	-3.39
	2	ω_{21}	3.71	3.8	-2.36
		ω_{22}	10.1	10.7	-5.60
	3	ω_{31}	6.99	7.2	-2.91
		ω_{32}	11.01	12.3	-10.48
$L/d_2=20$	1	ω_{11}	0.36	0.35	2.85
		ω_{12}	10.11	10.2	-0.88
	2	ω_{21}	0.98	1.0	-2.00
		ω_{22}	10.31	10.2	1.07
	3	ω_{31}	1.88	1.9	-1.05
		ω_{32}	10.64	10.3	3.30
$L/d_2=50$	1	ω_{11}	0.06	0.06	0.00
		ω_{12}	10.13	10.2	-0.68
	2	ω_{21}	0.16	0.16	0.00
		ω_{22}	10.32	10.2	1.17
	3	ω_{31}	0.31	0.31	0.00
		ω_{32}	10.41	10.2	2.05

Table XVI Frequencies of fixed DWNT (with inner diameter 0.7 nm. and the outer diameter 1.4 nm)

Cases	Modes		FE Model Frequency (THz)	Single Beam Theory (THz)	% of Error
$L/d_2=10$	1	ω_{11}	1.39	1.39	0.00
	2	ω_{21}	3.71	3.84	-3.38
	3	ω_{31}	6.99	7.54	-7.29
$L/d_2=20$	1	ω_{11}	0.36	0.35	2.85
	2	ω_{21}	0.98	0.96	2.08
	3	ω_{31}	1.88	1.88	0.00
$L/d_2=50$	1	ω_{11}	0.06	0.06	0.00
	2	ω_{21}	0.16	0.15	6.66
	3	ω_{31}	0.31	0.30	3.33

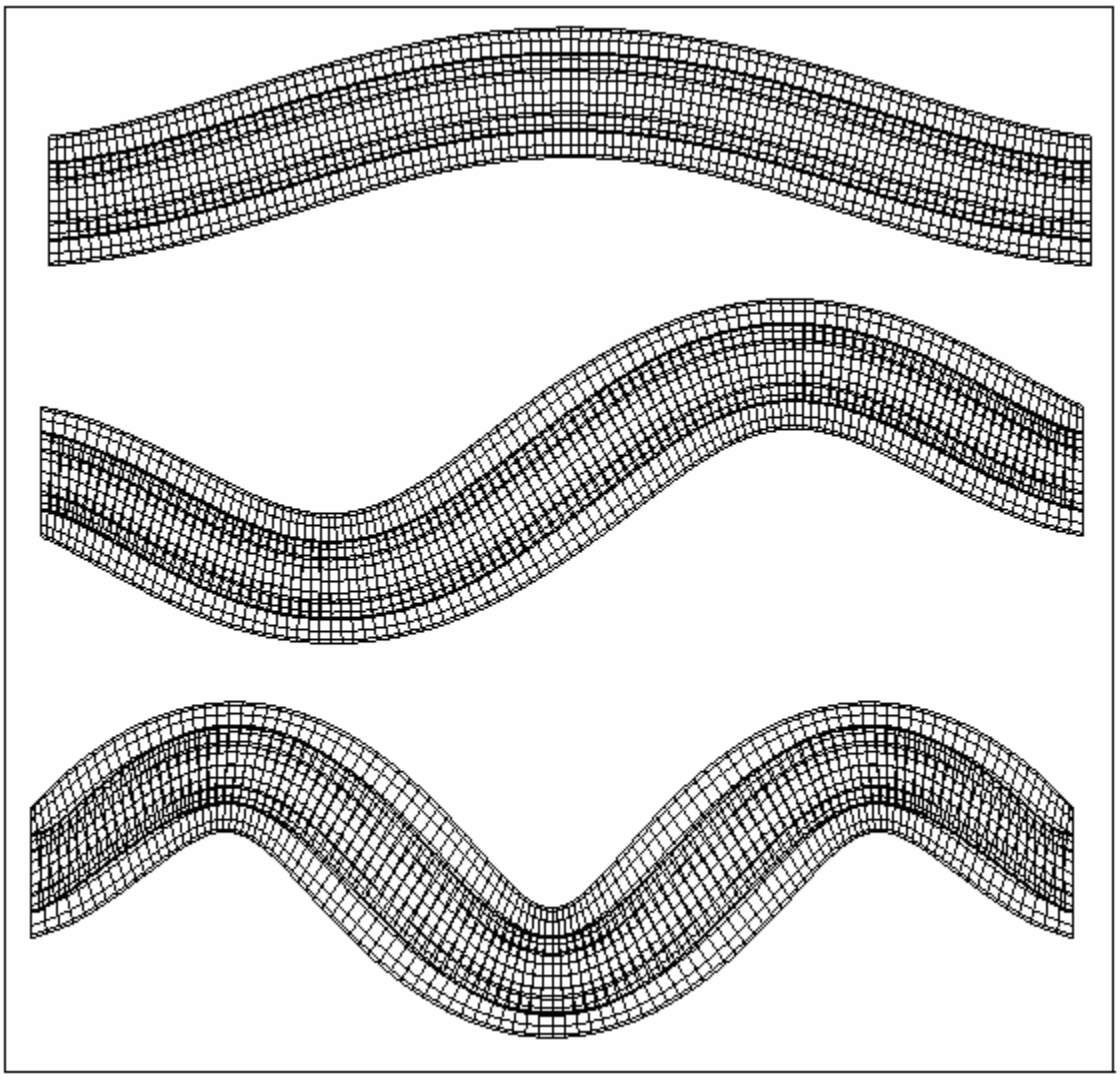

Figure XVI First three modes of fixed - fixed double walled carbon nanotube

Table XVII Frequencies of cantilever DWNT (with inner diameter 0.7nm and outer diameter 1.4nm

Cases	Modes		FE Model Frequency (THz)	J. Yoon[9] (THz)	% of Error
L/d_2=10	1	ω_{11}	0.22	0.22	0.00
		ω_{12}	9.51	10.2	-6.76
	2	ω_{21}	1.38	1.4	-1.42
		ω_{22}	9.53	10.3	-7.47
	3	ω_{31}	3.67	3.8	-3.42
		ω_{32}	9.59	10.7	-10.37
L/d_2=20	1	ω_{11}	0.06	0.06	0.00
		ω_{12}	10.2	10.2	0.00
	2	ω_{21}	0.35	0.35	0.00
		ω_{22}	10.5	10.2	2.94
	3	ω_{31}	0.99	1	-1.00
		ω_{32}	10.6	10.2	3.92
L/d_2=50	1	ω_{11}	0.01	0.01	0.00
		ω_{12}	10.2	10.2	0.00
	2	ω_{21}	0.06	0.06	0.00
		ω_{22}	10.4	10.2	1.96
	3	ω_{31}	0.16	0.16	0.00
		ω_{32}	10.4	10.2	1.96

Table XVIII Frequencies of Cantilever DWNT (with inner diameter 0.7 nm. and the outer diameter 1.4 nm)

Cases	Modes		FE Model Frequency (THz)	Single Beam Theory] (THz)	% of Error
L/d_2=10	1	ω_{11}	0.22	0.22	0.00
	2	ω_{21}	1.38	1.38	0.00
	3	ω_{31}	3.67	3.85	-4.67
L/d_2=20	1	ω_{11}	0.06	0.06	0.00
	2	ω_{21}	0.35	0.34	2.94
	3	ω_{31}	0.99	0.96	3.12
L/d_2=50	1	ω_{11}	0.01	0.01	0.00
	2	ω_{21}	0.06	0.06	0.00
	3	ω_{31}	0.16	0.15	6.66

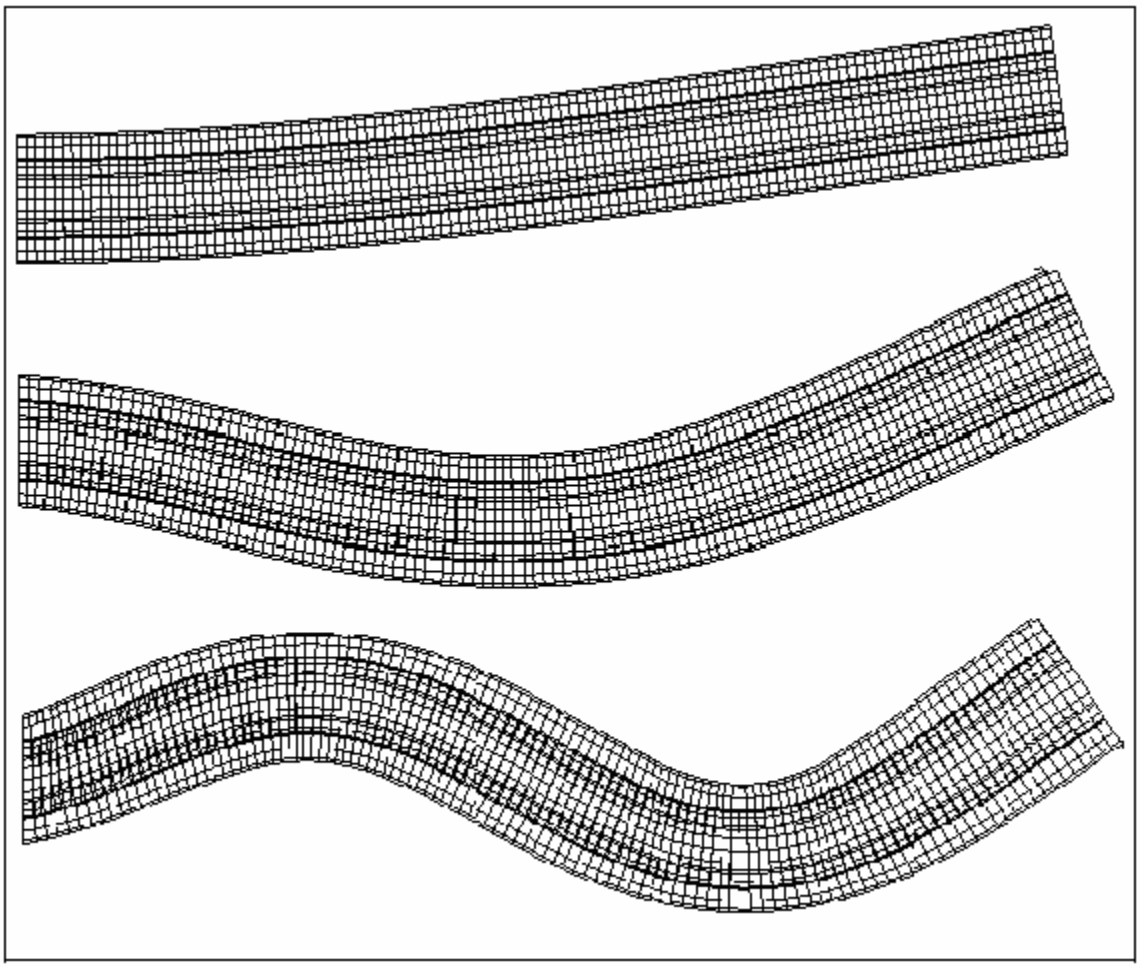

Figure XVII First three modes of cantilevered double walled carbon nanotube

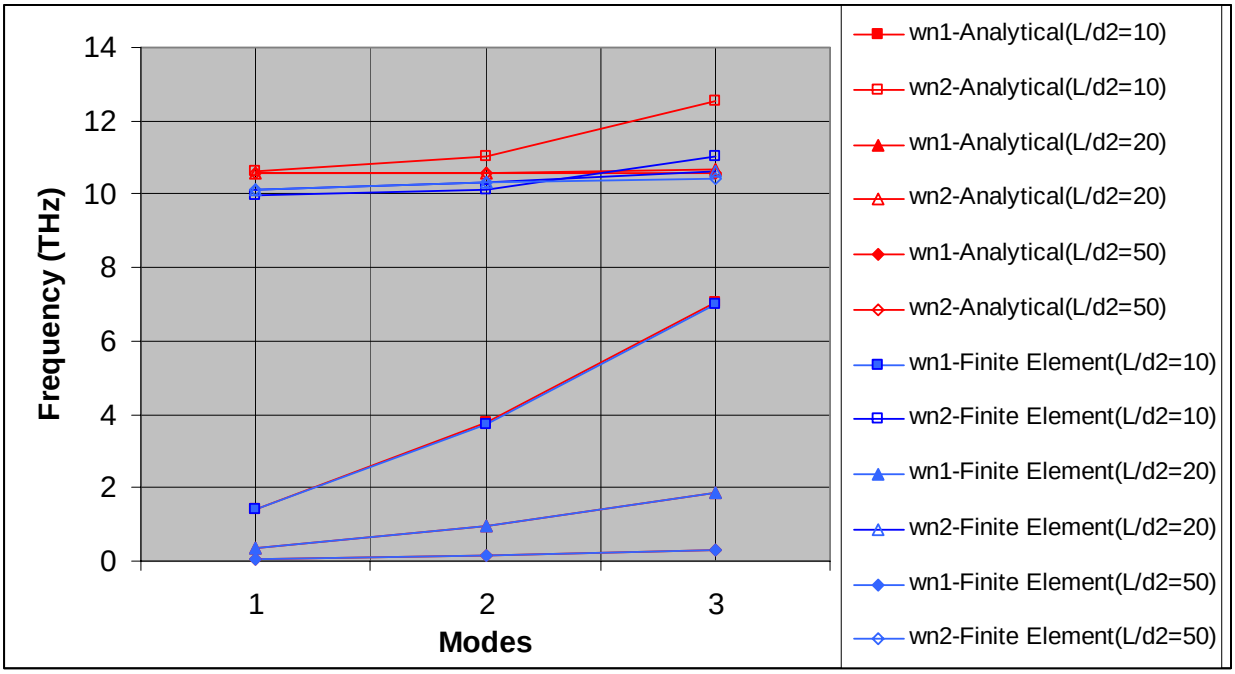

Figure XVIII Frequencies of Fixed DWNT (with inner diameter 0.7 nm. and the outer diameter 1.4 nm)

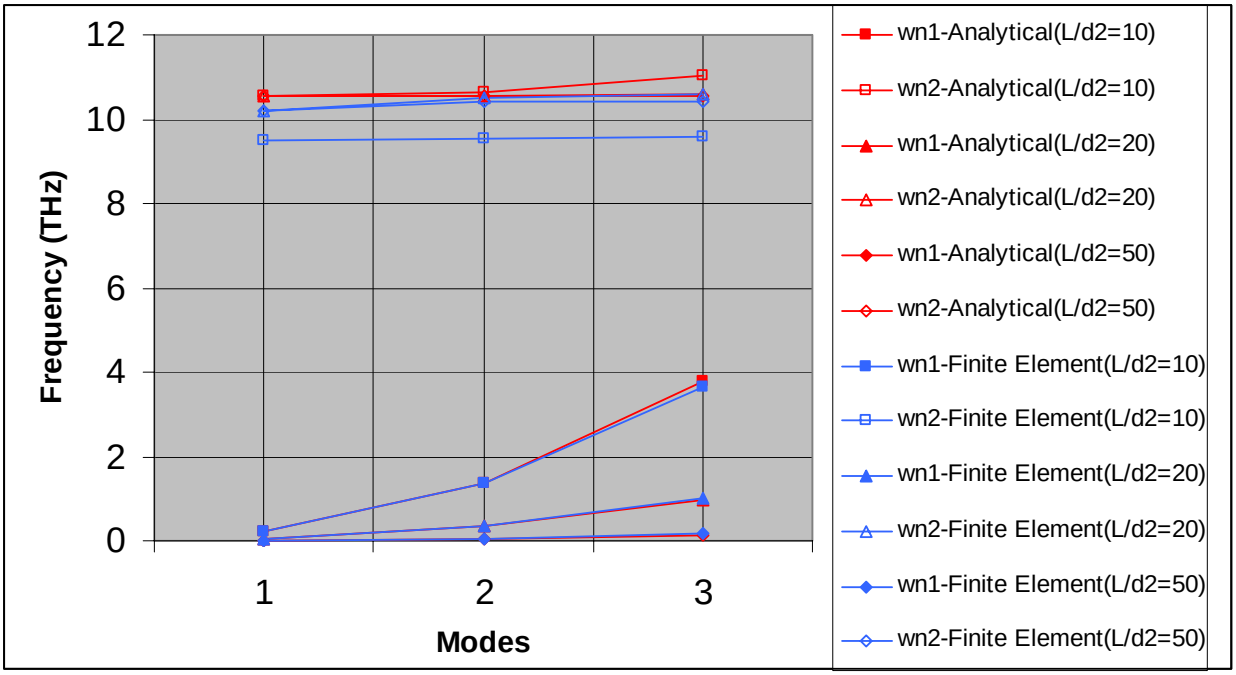

Figure XIX Frequencies of Cantilever DWNT (with inner diameter 0.7 nm. and the outer diameter 1.4 nm)

Table XVIII shows the frequencies of fixed DWNT with $d_1 = 0.7nm$ and $d_2 = 1.4nm$ for different aspect ratios. Table XIX shows the frequencies of cantilever DWNT with $d_1 = 0.7nm$ and $d_2 = 1.4nm$ for different aspect ratios. It is seen from tables XVIII and XIX that the lowest intertube frequencies are almost same for fixed DWNT and cantilever DWNT indicating that they are insensitive to the end conditions as predicted by Yoon et al. (2002). The first three intertube frequencies are around 10 THz as predicted by Yoon et al. (2002). The intertube resonant frequency (ωn1) is insensitive to the mode number and is much higher than the lowest natural frequency (ωn0) for larger aspect ratio's as predicted by Yoon et al. (2002). The percentage of error between continuum method and Yoon et al. (2002) and for lowest natural frequency (ωn0) is almost negligible. The percentage of error between finite element

results for both cantilever DWNT and fixed DWNT with J. Yoon [9] is very high [up to 10%] for small aspect ratios ($L/d_2 \leq 10$). The percentage of error for larger aspect ratio's are within 3 %.This result is also in agreement with Harik et al. (2002) who said that beam models can be used only if $L/d > 10$ .The finite element frequency for both cantilever DWNT's and fixed DWNT's where almost the same frequency of Yoon et al. (2002) for first mode for all aspect ratios.

The FE model results are also compared with single beam theory. The frequency of single beam theory for a DWNT is given by equation (150). Tables XVI and XVIII show the difference between DWNT finite element and single beam theory frequencies. The difference clearly shows the effect of van der Waals force on vibration of nanotube and the effect is high (up to 7 %) for smaller aspect ratios. For aspect ratios $L/d_2 \geq 50$, the difference between DWNT frequency and single beam theory frequency is almost zero indicating that effect of van der Waals force on vibration of nanotube is negligible for larger aspect ratios. The other interesting result is there is no effect for the first mode shape in all aspect ratios.

Figures XVIII shows the comparison of continuum model and finite element model frequencies of fixed DWNT. It can be seen that finite element model frequencies and continuum model frequencies are in good agreement for inner tube. Figures XIX shows the comparison of continuum model and finite element model frequencies of cantilever DWNT. It can be seen that finite element model frequencies and continuum model frequencies are in good agreement for inner tube.

Table XIX Frequencies of five walled nanotube (with inner diameter 0.7 nm and the outer diameter 3.5 nm)

Cases	Modes		FE Model Frequency (THz)	J. Yoon (2002) (THz)	% of Error
$L/d_5 = 10$	1	ω_{11}	0.45	0.49	-8.16
		ω_{12}	4.89	5.30	-7.73
		ω_{13}	8.40	9.00	-6.66
		ω_{14}	12.76	12.2	4.59
		ω_{15}	13.44	14.5	-7.31
$L/d_5 = 20$	1	ω_{11}	0.12	0.12	0.00
		ω_{12}	5.43	5.30	2.45
		ω_{13}	9.34	9.00	3.77
		ω_{14}	12.55	12.1	3.71
		ω_{15}	14.96	14.5	3.17
$L/d_5 = 5\ 0$	1	ω_{11}	0.02	0.02	0.00
		ω_{12}	5.41	5.30	2.07
		ω_{13}	9.21	9.00	2.33
		ω_{14}	12.43	12.1	2.72
		ω_{15}	14.71	14.5	1.44

Table XX Frequencies of five walled nanotube (with inner diameter 0.7 nm and the outer diameter 3.5 nm)

Cases	Modes		FE Model Frequency (THz)	Single Beam Theory (THz)	% of Error
$L/d_5 = 10$	1	ω_{11}	0.45	0.59	-23.72
		ω_{12}	4.89		
		ω_{13}	8.40		
		ω_{14}	12.76		
		ω_{15}	13.44		
$L/d_5 = 20$	1	ω_{11}	0.12	0.14	-14.28
		ω_{12}	5.43		
		ω_{13}	9.34		
		ω_{14}	12.55		
		ω_{15}	14.96		
$L/d_5 = 50$	1	ω_{11}	0.02	0.02	0.00
		ω_{12}	5.41		
		ω_{13}	9.21		
		ω_{14}	12.43		
		ω_{15}	14.71		

Table XXI Frequencies of five walled nanotube (with inner diameter 0.7 nm and the outer diameter 3.5 nm)

Cases	Modes		FE Model Frequency (THz)	Continuum Model Frequency (THz)	% of Error
$L/d_5 = 10$	1	ω_{11}	0.45	0.49	-8.16
		ω_{12}	4.89	5.45	-10.2
		ω_{13}	8.40	9.36	-10.2
		ω_{14}	12.76	12.5	2.08
		ω_{15}	13.44	14.9	-9.79
$L/d_5 = 20$	1	ω_{11}	0.12	0.12	0.00
		ω_{12}	5.43	5.43	0.00
		ω_{13}	9.34	9.35	-0.10
		ω_{14}	12.55	12.5	0.40
		ω_{15}	14.96	14.9	0.40
$L/d_5 = 5\ 0$	1	ω_{11}	0.02	0.02	0.00
		ω_{12}	5.41	5.43	-0.36
		ω_{13}	9.21	9.35	-1.49
		ω_{14}	12.43	12.5	-0.56
		ω_{15}	14.71	14.9	-1.27

Table XIX shows the finite element results for fixed five-walled nanotube in comparison with Yoon et al. (2002). The percentage of error is high (up to 8 %) for smaller aspect ratio ($L/d_5 = 10$). The percentage of error decreased as aspect ratio increased. Table XX shows the difference in frequencies of fixed five-walled nanotube and single beam theory. The van der Waals force has decreased the frequency of nanotube by 23 % for aspect ratio ($L/d_5 = 10$). This effect decreases as the aspect ratio increases. There is no effect of van der Waals force on vibration of nanotube of aspect ratio $L/d_5 \geq 50$. Table XXI shows the comparison of continuum model frequencies and finite element model frequencies. The finite element model is in good agreement with continuum model for aspect ratios $L/d_5 = 20$ and $L/d_5 = 50$.

CHAPTER 6 CONCLUSION

A methodology for constructing continuum models and finite element models of single and multi walled CNTs for vibration analysis is presented and validated with the existing results in the literature. Both continuum models and finite element models are validated with reference to single beam theory. Since the percentage of error is negligible, the models are concluded as valid. The lowest intertube frequencies are insensitive to the end conditions. The first three intertube frequencies are around 10 THz. The intertube resonant frequency (ω_{n1}) is insensitive to the mode number and is much higher than the lowest natural frequency (ω_{n0}) for larger aspect ratios. The mode shapes of cantilever SWNT is similar to the mode shapes of any elastic cantilever beam. The mode shapes for DWNT are co-axial for the first three mode shapes.

In case of fixed DWNT, there is absolutely no effect of van der Waals force on vibration for the first vibration mode of all aspect ratios. Whereas in cantilever DWNT and fixed five walled nanotube there is considerable effect of van der Waals force for the first vibration mode of all aspect ratios. In case of fixed DWNT and cantilever DWNT, the effect of van der Waals force on vibration for higher aspect ratios ($L/D_{out}>=50$) is zero. Whereas in fixed five walled NT, there is considerable effect of van der Waals force for the aspect ratio ($L/D_{out}=50$). The effect of van der Waals force on vibration is high for aspect ratio ($L/D_{out}=10$) when compared to other aspect ratios respective of boundary conditions and number of layers. The effect of van der Waals force in case of fixed DWNT is large when compared to cantilever DWNT for all aspect ratios.

The effect of van der Waals force on vibration of five walled nanotube is much larger than DWNT for all aspect ratios.

In summary, the effect of van der Waals force is high for

- Smaller aspect ratios irrespective of boundary conditions and number of layers.
- Fixed nanotube than cantilever nanotube for the same dimensions.
- Five-walled nanotube than a double walled nanotube for the same aspect ratio.

CHAPTER 7 FUTURE WORK

In the proposed finite element model the van der Waals force are represented by distributed springs and van der Waals force remains constant during deformation which is not in actual case. In future van der Waals force can be modeled as a pressure, approximated to be a linear function of change in inter-layer spacing.

Abaqus user subroutine UINTER suggested by Pantano et al. (2003) can be used to define the constitutive interaction between two deforming surface. Master and slaves surfaces are defined and the subroutine is alled for each slave node at each time increment of the analysis. Inputs to the subroutine are the initial and incremental relative positions of each slave node with respect to its closest point on the master surface, and any material properties defined by the user.

REFERENCES

1. Wang, Q., Varadan, V.K., 2005. Stability analysis of carbon nanotubes via continuum models. Smart Materials and Structures 14, 281.
2. Wang, Q., Hu, T., Chen, G., Jing, Q., 2005. Bending instability characteristics of Double walled carbon nanotubes. Physical Review B 71,045403.
3. Wang, Q., 2006. Wave propagation in carbon nanotubes via non-local continuum mechanics. Journal of Applied Physics. (In press).
4. Wang, Q., Varadan, V.K., 2005. Stability analysis of carbon nanotube probes for atomic force microscopy via continuum models. Smart Materials and Structures 14, 1196.
5. Wang, Q., 2005. Effect of van der Waals interaction on analysis of double walled carbon nanotubes. International Journal of Structural Stability and Dynamics 5(3) 457.
6. Wang, Q., Varadan, V.K., 2005. Wave characteristics of carbon nanotubes. International Journal of Solids and Structures (In press).
7. Wang, Q., Xu, F., and Zhou, G.Y., 2005. Continuum model for the stability analysis of carbon nanotubes under initial bend. International Journal of Structural Stability and Dynamics (In press).
8. Wang, Q., 2004. Effective in-plane stiffness and bending rigidity of armchair and zigzag carbon nanotubes. International Journal of Solids and Structures 41, 5451.

9. Wang, X., Wang, X.Y., Xiao, J., 2004. A Non-linear analysis of the bending modulus of carbon nanotubes with rippling deformations. Composite Structures, Article in press.
10. Pantano, A., Boyce, M.C., Perks, D.M., 2003. Non-linear structural mechanics based modeling of CNT deformation. Physical Review Letter, 91, 145504.
11. Poncharal, P., Wang, Z.L., Ugarte, D., De Heer, W.A., 1999. Electrostatic deflections and electromechanical resonances of CNTs. Science 283, 1513.
12. Krishnan, A., Dujardin, E., Ebbesen, T., Vianlias, P.N., Treacy, M.M.J., 1998. Young's modulus of single walled nanotubes, Physical Review B 58, 14043.
13. Huang, X.M.H., Zorman, C.A., Mehregany, M., Roukes, M.L., 2003. Nanodevice Motion at Microwave Frequencies, Nature 421, 496.
14. Liu, J.Z., Zheng, Q., and Jiang, Q., 2001. Effect of a rippling mode on resonances of carbon nanotubes. Physical Review Letters 86, No: 21, 4843.
15. Yoon, J., Ru, C., Mioduchowski, A., 2002. Noncoaxial resonance of an isolated multiwall CNT. Physical Review B 66, 233402.
16. Ru, C., 2000. Effect of van der Waals force on axial buckling of a double walled CNT. Journal of Applied Physics 87(10), 7227.
17. Harik, V.M., 2002. Mechanics of carbon nanotubes: applicability of the continuum-beam models. Computational Materials Science 24, 328.
18. Govindjee, S., Sackman, J.L., 1999. On the use of continuum mechanics to estimate the properties of nanotubes. Solid State Communications 110, 227.
19. Snow, E.S., Campbell, P.M., Novak, J.P., 2002. Single wall carbon nanotube force microscope probes. Applied Physics Letter 80(11).

20. Ru, C., 2000. Column buckling of multiwalled carbon nanotubes with interlayer radial displacements, Physical Review B 62 (24), 16962.
21. Girifalco L.A., Lad R.A., 1956. Energy of Cohesion, Compressibility, and the Potential Energy Functions of the Graphite System, Journal of Chemical Physics 25, 693.
22. Yakobson B.I., Brabec C.J., Bernholc J., 1996. Nanomechanics of Carbon Tubes: Instabilities beyond Linear response, Physical Review Letters 76(14), 2511.
23. Ajayan M., Zhou O.Z., 2001. Applications of Carbon Nanotubes, Applied Physics 80,391.
24. Gao B., 2000. Chemical Physics. Enhanced Saturation Lithium Composition in Ball-Milled Single Walled Carbon Nanotubes. Chemical Physics Letters 327, 69.
25. ABAQUS Documentation set.
26. http://www.pa.msu.edu/cmp/csc/nanotube.html
27. http://en.wikipedia.org/wiki/Carbon_nanotube
28. http://www.azonano.com/details.asp?ArticleID=1108